blood®
Regular Article

MYELOID NEOPLASIA

Disruption of dNTP homeostasis by ribonucleotide reductase hyperactivation overcomes AML differentiation blockade

Hanying Wang,[1,2,*] Xin He,[1,*] Lei Zhang,[1,*] Haojie Dong,[1] Feiteng Huang,[1,3] Jie Xian,[1] Min Li,[4] Wei Chen,[5] Xiyuan Lu,[6] Khyatiben V. Pathak,[7] Wenfeng Huang,[1] Zheng Li,[1,8] Lianjun Zhang,[1] Le Xuan Truong Nguyen,[1] Lu Yang,[9] Lifeng Feng,[10] David J. Gordon,[11] Jing Zhang,[12] Patrick Pirrotte,[7,13] Chun-Wei Chen,[9] Amandeep Salhotra,[14] Ya-Huei Kuo,[1] David Horne,[15] Guido Marcucci,[1,14] David B. Sykes,[16] Stefano Tiziani,[6,17,18] Hongchuan Jin,[10,†] Xian Wang,[2,†] and Ling Li[1,†]

[1]Department of Hematological Malignancies Translational Science, Gehr Family Center for Leukemia Research, Hematologic Malignancies and Stem Cell Transplantation Institute, Beckman Research Institute, City of Hope Medical Center, Duarte, CA; [2]Department of Medical Oncology and [3]Department of Hematology, Sir Run Run Shaw Hospital, Zhejiang University, Hangzhou, China; [4]Department of Information Sciences, Beckman Research Institute and [5]Integrative Genomics Core, Beckman Research Institute, City of Hope Medical Center, Duarte, CA; [6]Department of Nutritional Sciences, The University of Texas at Austin, Austin, TX; [7]Cancer & Cell Biology Division, The Translational Genomics Research Institute, Phoenix, AZ; [8]Department of Hematology, The First Affiliated Hospital of Soochow University, Suzhou, China; [9]Department of Systems Biology, Beckman Research Institute, City of Hope Medical Center, Duarte, CA; [10]Laboratory of Cancer Biology, Provincial Key Laboratory of Biotherapy in Zhejiang, Sir Run Run Shaw Hospital, Zhejiang University, Hangzhou, China; [11]Division of Pediatric Hematology/Oncology, Department of Pediatrics, University of Iowa, Iowa City, IA; [12]McArdle Laboratory for Cancer Research and Wisconsin Blood Cancer Research Institute, University of Wisconsin-Madison, Madison, WI; [13]Cancer & Cell Biology Division, The Translational Genomics Research Institute, Phoenix, AZ; [14]Department of Hematology and Hematopoietic Cell Transplantation and [15]Department of Molecular Medicine, Beckman Research Institute of City of Hope, Duarte, CA; [16]Center for Regenerative Medicine, Massachusetts General Hospital, Boston, MA; and [17]Department of Pediatrics and [18]Department of Oncology, Dell Medical School, LiveSTRONG Cancer Institutes, The University of Texas at Austin, Austin, TX

KEY POINTS

- **RNR hyperactivation disrupts dNTP homeostasis, promoting myeloid differentiation in AML.**
- **dNTP pool imbalance induces excessive ERK activation, contributing to leukemia cell differentiation/viability inhibition outcome.**

Differentiation blockade is a hallmark of acute myeloid leukemia (AML). A strategy to overcome such a blockade is a promising approach against the disease. The lack of understanding of the underlying mechanisms hampers development of such strategies. Dysregulated ribonucleotide reductase (*RNR*) is considered a druggable target in proliferative cancers susceptible to deoxynucleoside triphosphate (dNTP) depletion. Herein, we report an unanticipated discovery that hyperactivating RNR enables differentiation and decreases leukemia cell growth. We integrate pharmacogenomics and metabolomics analyses to identify that pharmacologically (eg, nelarabine) or genetically upregulating RNR subunit M2 (*RRM2*) creates a dNTP pool imbalance and overcomes differentiation arrest. Moreover, R-loop–mediated DNA replication stress signaling is responsible for RRM2 activation by nelarabine treatment. Further aggravating dNTP imbalance by depleting the dNTP hydrolase SAM domain and HD domain-containing protein 1 (*SAMHD1*) enhances ablation of leukemia stem cells by RRM2 hyperactivation. Mechanistically, excessive activation of extracellular signal-regulated kinase (*ERK*) signaling downstream of the imbalance contributes to cellular outcomes of RNR hyperactivation. A CRISPR screen identifies a synthetic lethal interaction between loss of *DUSP6*, an ERK-negative regulator, and nelarabine treatment. These data demonstrate that dNTP homeostasis governs leukemia maintenance, and a combination of DUSP inhibition and nelarabine represents a therapeutic strategy.

Introduction

Acute myeloid leukemia (AML) is characterized by differentiation arrest within bone marrow (BM).[1,2] Successful use of all-trans retinoic acid (ATRA) or inhibitors of mutant isocitrate dehydrogenase (IDH) highlights the achievement of differentiation therapy.[3-5] Other differentiating compounds whose effects are not limited to any specific leukemia subtype are those intervening nucleotide metabolism, including nucleoside analogs (eg, Ara-C)[6] or inhibitors of dihydroorotate dehydrogenase.[7] There is an unmet need to understand mechanisms underlying activity of those agents.

Proliferative cancer cells hijack de novo deoxynucleoside triphosphate (dNTP) biosynthesis to meet DNA replication demands.[8] A key player in dNTP biosynthesis is ribonucleotide reductase (RNR).[9] The functional RNR catalytic unit is a cytosolic heterotetramer consisting of 2 large subunits (RRM1) and 2 small

subunits (RRM2 and RRM2B).[9] RRM2 levels vary throughout the cell cycle; its transcription is minimal in G_0/G_1 and maximal in S phase, determining RNR activity.[10-12] RRM2 levels are tightly regulated by the DNA damage-induced ataxia telangiectasia and Rad3-related (*ATR*) pathway,[13,14] which is downstream of augmented R-loops, the triple-stranded DNA:RNA hybrids.[15,16] Moreover, high dNTP levels are reportedly mutagenic via perturbing DNA replication and impairing mitochondrial function.[17] The dNTP hydrolase SAM domain and HD domain-containing protein 1 (SAMHD1), which degrades dNTP and functionally antagonizes RNR,[17-19] reportedly promotes resistance to nucleoside-based chemotherapies by hydrolyzing active triphosphate metabolites like Ara-CTP.[20,21] Last, RNR activation may have opposing effects on tumorigenesis,[22] prompting us to explore the role of RNR hyperactivation in AML.

Herein, we identify nelarabine (NEL) from our differentiation compound screen. Its effects stem from R-loop–mediated replication stress and RNR hyperactivation-induced dNTP imbalance. We further characterize extracellular signal-regulated kinase (ERK) hyperactivation as downstream of the imbalance.

Methods

Patient samples

Peripheral blood or BM specimens were obtained from patients with AML at City of Hope (COH) Comprehensive Cancer Center. Patient characteristics are summarized in supplemental Table 4 available at the *Blood* Web site. Risk groups are based on World Health Organization classification. All subjects signed informed consent forms. Sample acquisition was approved by COH Institutional Review Board in accordance with the Declaration of Helsinki.

Mice

Immunodeficient NOD-scid IL2Rgnull-3/GM/SF (NSGS) mice used for human-in-mouse xenograft models were obtained from the Jackson Laboratory (stock no. 013062). *Mll-AF9/Samhd1*$^{-/-}$ mice were generated by crossing *Samhd1*$^{-/-}$ mouse[23] with *Mll-AF9* (MA9) knock-in mouse (Jackson Laboratory, stock no. 009079). CD45.1^{+} congenic mice were from the National Cancer Institute (strain no. 01B96). Mouse care and experimental procedures complied with established institutional guidance and approved protocols from the Institutional Animal Care and Use Committee at COH.

Metabolomic analysis

Metabolites were extracted with methanol and subjected to targeted metabolomic profiling on the UltiMate 3000 UPLC chromatography system coupled with Q-Exactive orbitrap mass spectrometer. Targeted metabolites were quantified by area under the curve (AUC). Other details are provided in supplemental Materials.

Mass cytometry

Primary cells were treated as indicated and processed according to the Fluidigm protocol. Other analysis procedures are provided in supplemental Methods.

RNA-Seq analysis

Total RNA was isolated from cells treated as indicated. RNA sequencing libraries preparation procedures are provided in supplemental Methods. Sequencing run was performed in the single read mode using Illumina HiSeq 2500.

Statistics

Data obtained from multiple experiments were reported as mean ± standard error of the mean (SEM). Unpaired, 2-sided Student *t* test was used to compare means between 2 groups. One-way analysis of variance with multiple comparisons was used to compare means among 3 or more groups.

Results

Functional screen reveals a differentiation-induction activity of NEL

To define potential differentiation indicators for virtual screen, analysis of GSE125112 revealed 35 genes commonly upregulated by ATRA[24] (fold-change ≥ 1.5; $P < .01$; Figure 1A; supplemental Table 1). In parallel, analysis of gene expression profiles of differentiation-inducing agents from NCI-60,[25] including ATRA, zalcitabine,[26] and sodium butyrate,[27] revealed 55 commonly upregulated genes ($r > 0.3$, $P < .01$; Figure 1A; supplemental Table 2). There was an overlap of only 1 gene, *CD38*, whose high expression is seen at later stages of hematopoietic differentiation.[28] Interestingly, transcriptome analysis of the lineage^{-}Sca^{+}cKit^{+} (LSK) subset sorted from conditional *Idh2*^{R140Q};*Flt3*^{ITD} knock-in mice revealed that *Cd38* was upregulated by in vivo administration of AG-221, a potent IDH2 inhibitor[29] (supplemental Figure 1A). We confirmed CD38 induction in U937, KG1A, and NB4 after ATRA, zalcitabine, or sodium butyrate treatment (supplemental Figure 1B) and *IDH2*^{R140Q}-expressing TF-1 after AG-221 treatment as reported[28] (supplemental Figure 1C).

We next queried the developmental therapeutics program database (>20 000 compounds) with *CD38* as input (Figure 1B). Among compounds retrieved from CellMiner,[25] 26 US Food and Drug Administration (FDA)-approved compounds were positively correlated with CD38 level ($r > 0.3$, $P < .01$), including ATRA (NSC-122758; $r = 0.543$, $P < .01$). We requested the top 79 compounds available from the National Cancer Institute ($r > 0.6$, $P = 0$) for phenotypic screen (Figure 1B; supplemental Table 3) using ER-HoxA9 cells, a murine differentiation-arrest model.[7] At a fixed dose of 5 μg/mL, 3 compounds (NSC-641818, NSC-37641, and NSC-755985 [NEL]) exhibited remarkable differentiation (GFP^{+} percentage >25%; Figure 1C). NEL was the only FDA-approved compound identified.[30-34] Following NEL treatment, ER-HoxA9 cells underwent neutrophil-like changes (Figure 1D).

We next determined whether NEL promoted differentiation in human AML. NEL treatment upregulated myeloid marker expression levels within a clinically achievable concentration[35] (Figure 1E-F; supplemental Figure 1D-E; supplemental Table 4). NEL-treated cells also showed cytochemical changes and cellular morphology suggestive of neutrophil or monocyte maturation[36] (Figure 1G; supplemental Figure 1F). NEL treatment upregulated levels of transcription factors associated with myeloid differentiation[37] (Figure 1H), eventually resulting in apoptosis and growth inhibition (supplemental Figure 1G-H). NEL's differentiation induction effects were correlated with viability inhibition in AML cells (supplemental Figure 1I-J); the treatment had less effects on viability of normal CD34^{+} cells

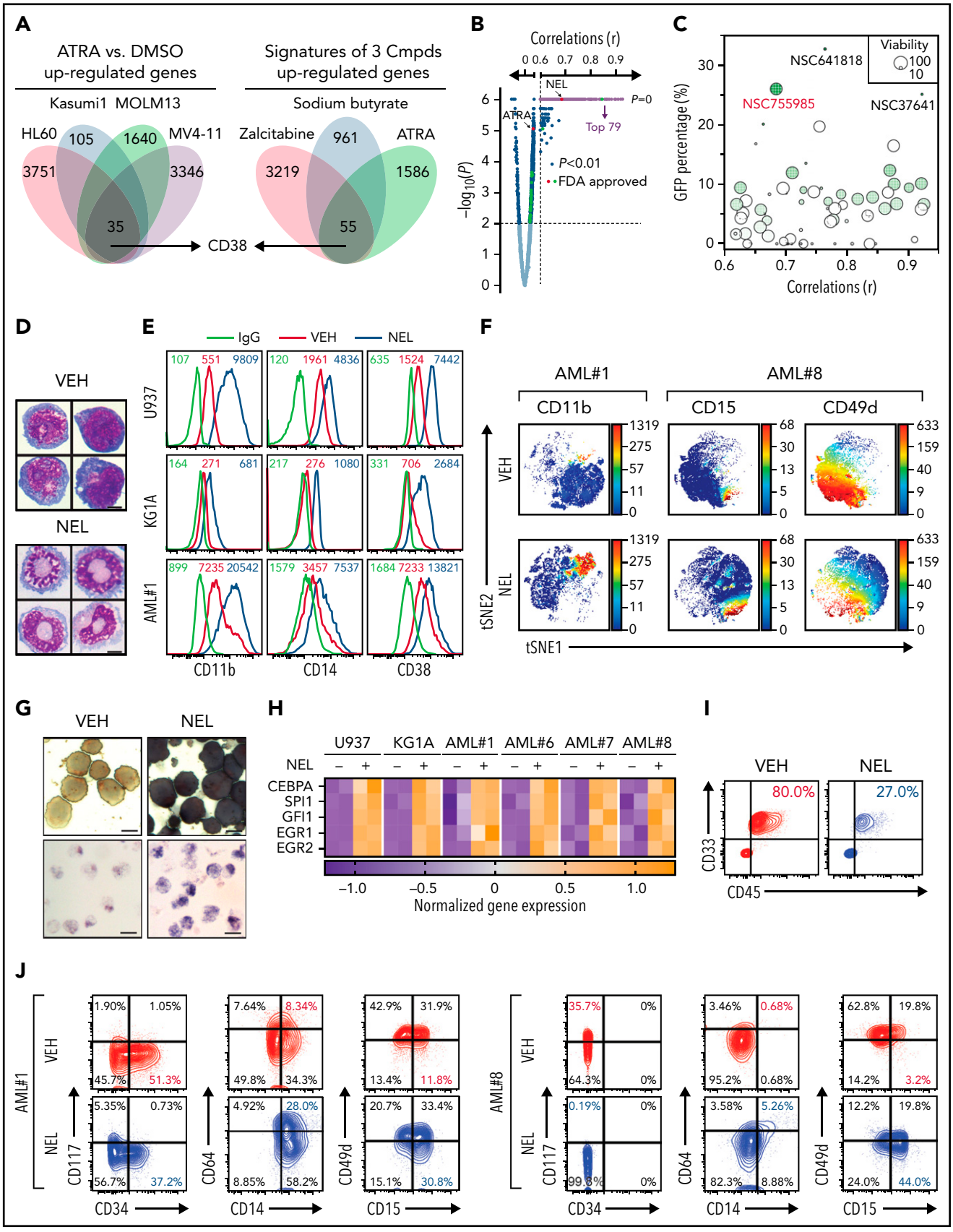

Figure 1. Functional screen reveals a differentiation-induction activity of nelarabine. (A) Venn plots depicting the approach to identify a differentiation marker by integrative analyses of GSE125112 dataset and CellMiner. Thirty-five genes were identified as overlapped upregulated genes after ATRA treatment in 4 AML lines (i); 55 genes were identified as overlapped upregulated genes among 3 differentiation-induction agents mediated gene expression profiles (ii). *CD38* is the only overlapped gene from 2 lists. (B) Volcano plot showing Pearson correlations vs -Log_{10} *P* values for all compounds retrieved from CellMiner with *CD38* as input. FDA-approved compounds are highlighted in green. Isotretinoin (ATRA) and nelarabine (NEL) are highlighted in red. Among the top 193 compounds ($r > 0.6$, $P = 0$,

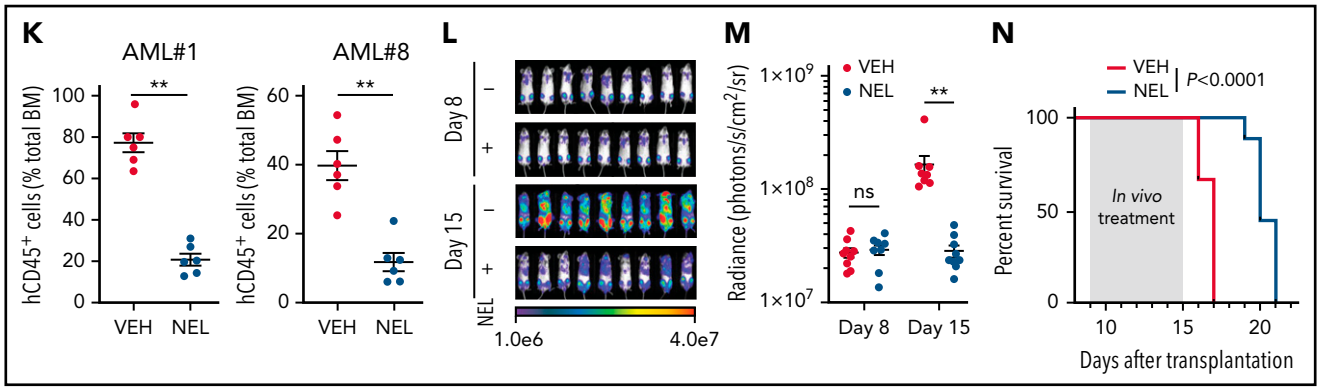

Figure 1 (continued) highlighted in purple), 79 available compounds were requested for further analysis. (C) Effects of 79 compounds on differentiation assessed by green fluorescent protein percentage in ER-HoxA9 cells. The diameter indicates the relative cell viability. Nelarabine (NSC755985) is highlighted in red. (D) Representative morphologic changes in ER-HoxA9 cells that accompanied myeloid differentiation shown by Wright-Giemsa staining of cells in the presence and absence of nelarabine treatment (10 μM, 96 hours). Scale bar, 5 μm. (E) Expression levels of surface markers CD11b, CD14, and CD38 in indicated cell lines and primary AML CD34$^+$ cells (AML#1) after NEL treatment (U937, KG1A, 10 μM, 96 hours; AML#1, 20 μM, 96 hours). Mean fluorescence intensity is indicated in histograms. (F) Representative t-distributed stochastic neighbor embedding (tSNE) display of mass cytometry analyses of primary AML cells treated with NEL (20 μM, 96 hours), colored by expression of the indicated markers based on CD3$^-$CD19$^-$ subsets. (G) Representative cytochemical staining of U937 cells after NEL treatment (10 μM, 96 hours) assessed by monocyte-specific α-naphthyl acetate esterase assay (i) and nitroblue tetrazolium reduction assay (ii). Scale bar, 15 μm. (H) Heatmap showing expressions of myeloid transcription factors in indicated AML cells after NEL treatment (U937, KG1A, 10 μM, 48 hours; AML#1, AML#6, AML#7, AML#8, 20 μM, 48 hours). Gene expression levels shown in duplicates were first normalized to GAPDH and then vehicle-treated cells. (I-K) Purified cells (1×10^6 cells per mouse) from primary specimens AML#1 (CD34$^+$ cells) and AML#8 (CD3$^+$ depleted cells) were injected into sublethally irradiated NSGS mice. Following confirmation of >1% engraftment in peripheral blood (PB), mice were treated with NEL (217 mg/kg, IV, daily) or vehicle (PBS) for 2 weeks (n = 6 mice per group). Human cell engraftment was analyzed 12 weeks after bone marrow transplantation (BMT). Representative CD45 and CD33 expression in BM of xenografts (I), immunophenotype of the primitive subpopulation (CD34$^+$ or CD117$^+$), monocyte subpopulation (CD14$^+$/CD64$^+$), and neutrophil subpopulation (CD15$^+$/CD49d$^-$) (J), and percentage of human CD45$^+$ cells in total BM (K) are shown. For panel K, results represent the mean ± SEM. $^{**}P < .01$. (L-N) U937-lucifase cells (0.5×10^6 cells per mouse) were injected into sublethally irradiated NSGS mice. Following engraftment confirmation, mice were treated with NEL (217 mg/kg, IV, daily) or vehicle (PBS) for 7 days (n = 9 per group) and then assessed for engraftment by in vivo bioluminescence imaging (L). Quantitative results from bioimaging (M) and mice survival after treatment discontinuation (N) are shown. For panel M, results represent mean ± SEM. ns, nonsignificant; $^{**}P < .01$.

(supplemental Figure 1I). Moreover, colony-formation capacity (CFC) of AML cells was suppressed (supplemental Figure 1K).

To evaluate in vivo effects of NEL treatment, we injected CD34$^+$ or T cell–depleted AML cells into NSGS mice[38] (supplemental Figure 1L). NEL treatment[39] significantly decreased leukemic cell engraftment (Figure 1I,K; supplemental Figure 1M). In vivo differentiation effects were confirmed (Figure 1J). Specifically, loss of the primitive subpopulation (CD117$^+$ or CD34$^+$) and emergence of monocyte or neutrophil subpopulation (CD14b$^+$/CD64$^+$ or CD15$^+$/CD49d$^-$) were seen. We further extended our study to NSGS mice xenografted with U937 cells. Importantly, NEL administration significantly delayed leukemia onset and conferred a survival advantage relative to controls (Figure 1L-N).

NEL's differentiation-induction is caused by dNTP imbalance

Ara-GTP is NEL's active metabolite[40,41] (supplemental Figure 2A). Accordingly, U937 cells that are more sensitive to NEL relative to THP1 accumulated higher levels of Ara-GTP after comparable treatment (supplemental Figures 1I and 2B). We hypothesized that NEL-induced differentiation was related to nucleotide metabolism perturbation. Metabolomic analysis of NEL-sensitive cells (U937 and KG1A) revealed that many deoxynucleotides increased to different extents after NEL treatment (Figure 2A; supplemental Figure 2C; supplemental Table 5). Moreover, the analyses were performed after treatment for 12 hours when the cell growth had not been altered yet (supplemental Figure 1H), suggesting that these changes were unlikely consequences of cell death. NEL treatment did not increase fractions of newly generated deoxynucleotides synthesized from glucose or glutamine (Figure 2B; supplemental Figure 2D; supplemental Tables 6-7), excluding the contribution of de novo synthesis.

Given that our initial metabolomics analysis cannot distinguish isobaric nucleotides, we performed a targeted nucleotide quantification assay to assess NEL treatment effects on a full panel of dNTPs/NTPs (Figure 2C-D; supplemental Figure 2E) and found that NEL treatment increased dNTP levels unequally. The resultant imbalance was featured by a dramatic increase in dGTP levels (Figure 2C-D; supplemental Figure 2F), in contrast to modest and symmetric increases of dNTPs during G_1/S transition when RNR activity increases[41-43] (supplemental Figure 2G-H).

We then asked whether the unequal increases in dNTPs and differentiation outcome were mediated by *RNR*. To test the possibility, we used an RNR inhibitor COH29, which targets the ligand-binding pocket of RRM2.[44] Supplementation with COH29 alleviated dNTP imbalance (Figure 2C-D; supplemental Figure 2F) and reversed differentiation after NEL exposure (Figure 2E-F). Similar rescue was seen after treatment of hydroxyurea (HU), another RNR inhibitor[45] (data not shown). Unlike short-term exposure (Figure 2C-D), long-term treatment of COH29 depleted dNTPs[44] (supplemental Figure 2I). Although COH29 treatment alone did not induce differentiation (supplemental Figure 2J), it did inhibit cell growth in both normal and AML cells (supplemental Figure 2K-L). To validate the viability rescue by diminishing dNTP imbalances, we established an "*RRM2*-low" line by introducing a doxycycline (DOX)-inducible *RRM2*-shRNA construct (ishRRM2) into U937 cells. DOX treatment decreased RRM2 protein levels by approximately 50% (Figure 2G), with minimal effects on cell cycling (supplemental Figure 2M). As anticipated, after NEL treatment, this line exhibited less dNTP imbalance (supplemental Figure 2N), differentiation

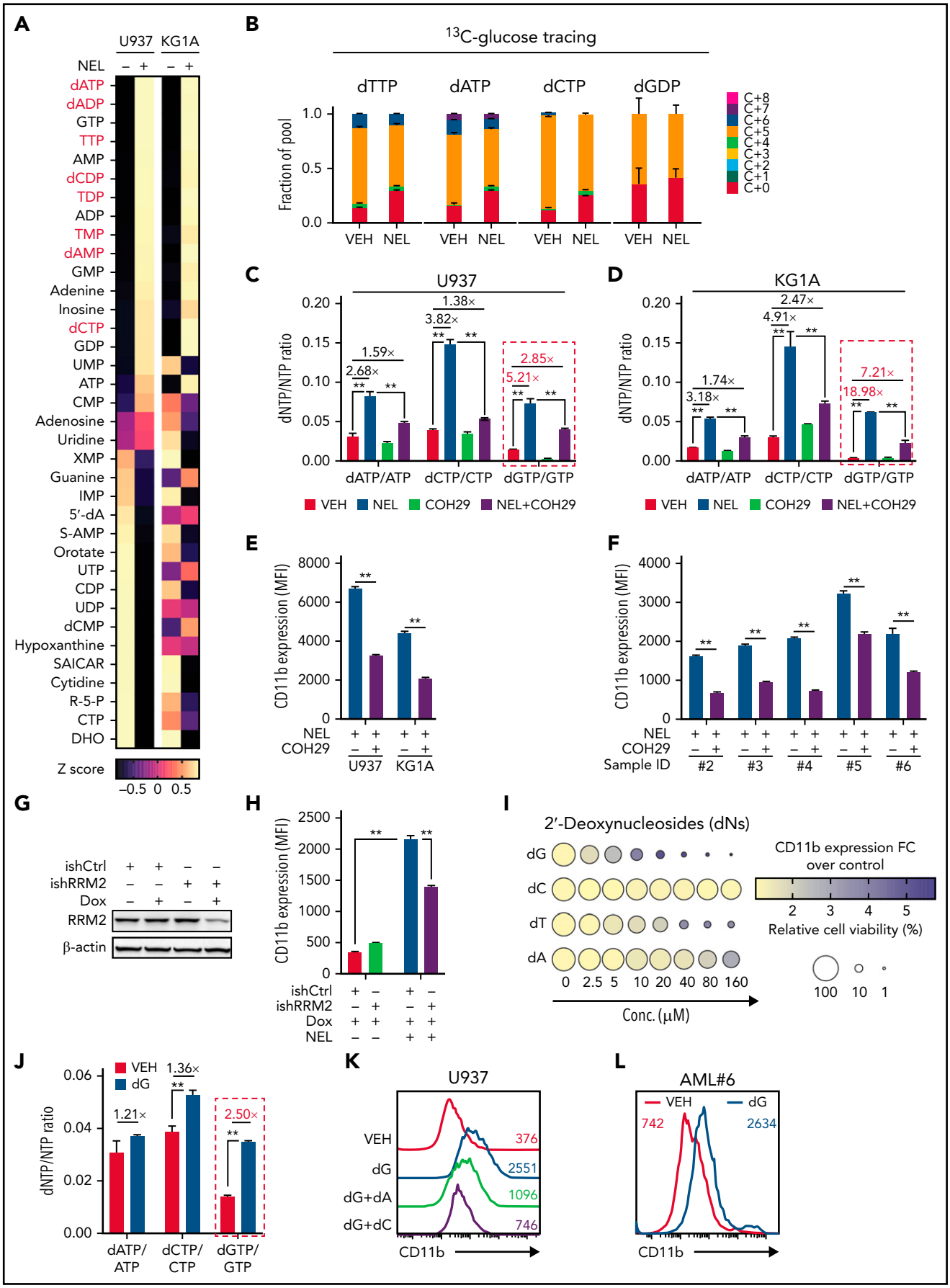

Figure 2. NEL's differentiation-induction is caused by dNTP imbalance. (A) Heatmaps showing changes of 36 intracellular nucleotide metabolites in U937 (i) or KG1A (ii) cells treated with vehicle or NEL (10 μM) for 12 hours. Commonly increased deoxynucleotides in both lines are highlighted in red. Data from duplicates are represented as Z-score–normalized intensities. (B) Fractional labeling of indicated deoxynucleotides in vehicle- or NEL-treated U937 cells cultured in media containing

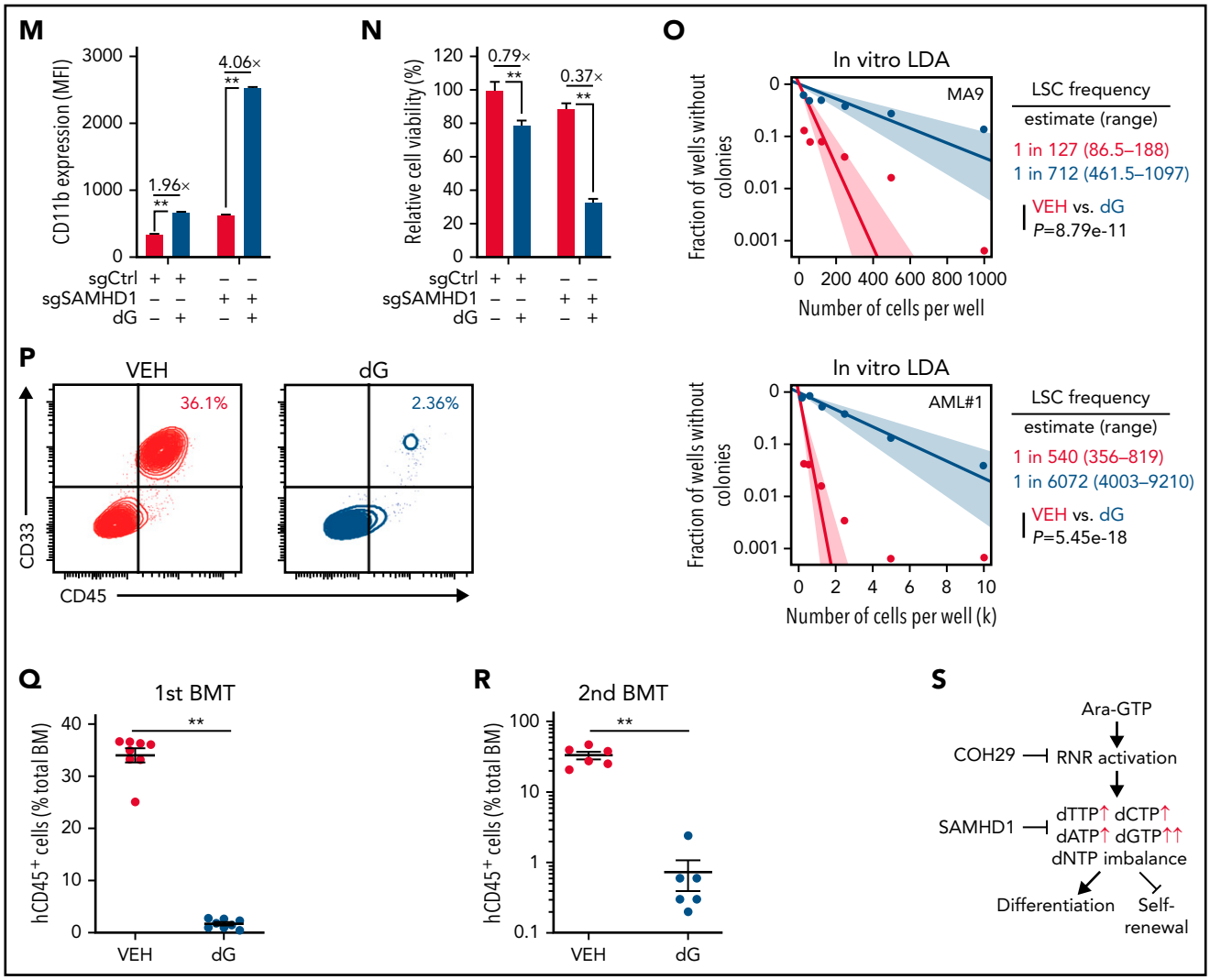

Figure 2 (continued) ^{13}C-labeled glucose for 12 hours. The color indicates different isotopologues. Data from triplicates are normalized to total amounts of individual deoxynucleotides and represented as mean ± SEM. (C-D) U937 (C) and KG1A (D) were treated with vehicle, NEL (10 μM), COH29 (10 μM), or combination for 12 hours, and intracellular dNTP levels were quantified relative to their NTP counterparts by high-performance liquid chromatography/mass spectrometry (HPLC/MS). Numbers denote the fold changes of dNTP/NTP ratios relative to vehicle-treated controls. Results represent the mean ± SEM. $^{**}P < .01$. (E-F) CD11b expression levels in indicated AML lines (E) or primary AML CD34$^+$ cells (F) treated with NEL (U937 and KG1A, 10 μM, 96 hours; primary AML cells, 20 μM, 96 hours) in the absence or presence of COH29 (10 μM). Results represent mean ± SEM. $^{**}P < .01$. (G) Western blot of RRM2 proteins in U937 cells transduced with inducible shRRM2 (ishRRM2) or shCtrl (ishCtrl) construct with or without doxycycline induction (2 μg/mL). (H) CD11b expression levels of ishCtrl- and ishRRM2-U937 cells with or without NEL treatment (10 μM, 96 hours) after doxycycline induction. Results represent mean ± SEM. $^{**}P < .01$. (I) Relative cell viability and CD11b expression levels of U937 cells treated with gradually increasing doses of deoxynucleosides (dA, dT, dC, dG) for 48 hours. The color represents CD11b expression fold changes over vehicle control; the diameter indicates the relative cell viability. (J) U937 cells were treated with vehicle or dG (10 μM) for 12 hours, and intracellular dNTP levels were quantified relative to their NTP counterparts by HPLC/MS. Numbers denote the fold changes of dNTP/NTP ratios relative to vehicle-treated controls. Results represent mean ± SEM. $^{**}P < .01$. (K) CD11b expression levels in U937 cells treated with vehicle, dG (10 μM), dG (10 μM) plus dA (10 μM), dG (10 μM) plus dC (10 μM) for 48 hours. (L) CD11b expression levels in primary AML CD34$^+$ cells from specimen AML#6 treated with vehicle or dG (15 μM, 48 hours). (M-N) CD11b expression levels (M) and relative cell viability (N) of sgCtrl- and sgSAMHD1-THP1 cells treated with vehicle or dG (15 μM, 48 hours). Numbers denote the fold changes relative to vehicle-treated controls. Results represent mean ± SEM. $^{**}P < .01$. (O) In vitro LDA assay showing LSC frequency changes in *MA9*$^+$ primary murine AML cells (i) and primary AML CD34$^+$ cells from specimen AML#1 (ii) after dG treatment (15 μM, 7 days). (P-R) Primary AML CD34$^+$ cells (1×10^6 cells per mouse) from specimen AML#1 were first treated with vehicle or dG (15 μM, 48 hours) ex vivo and then injected into sublethally irradiated NSGS mice (6-8 mice per group). Mice were killed 12 weeks after BMT for analysis of human cell engraftment, followed by secondary transplantation. Representative CD45 and CD33 expression in BM of primary transplants (P), percentage of human CD45$^+$ cells in BM of primary recipient mice (Q), and secondary recipient mice (R) are shown. For panels Q and R, results represent mean ± SEM. $^{**}P < .01$. (S) A working model depicting how dNTP imbalance overcomes differentiation blockade and impairs LSC self-renewal. As an active metabolite of NEL, Ara-GTP disrupts dNTP pool homeostasis through promoting RNR activity. COH29 treatment reverses the differentiation phenotype by inhibiting RNR activity, whereas *SAMHD1* antagonizes increases of dNTP levels.

(Figure 2H; supplemental Figure 2O), and viability inhibition (supplemental Figure 2P) than those seen in controls (ishCtrl).

We then tested whether supplementing cells with individual deoxynucleosides (dNs)[18] to experimentally create a dNTP imbalance would phenocopy NEL treatment, given that exogenous dNs can be salvaged to form dNTPs.[46] Indeed, dG treatment induced robust differentiation and cell death (Figure 2I; supplemental Figure 2Q). dT or dA treatment induced differentiation at relatively higher doses, whereas dC did not antagonize

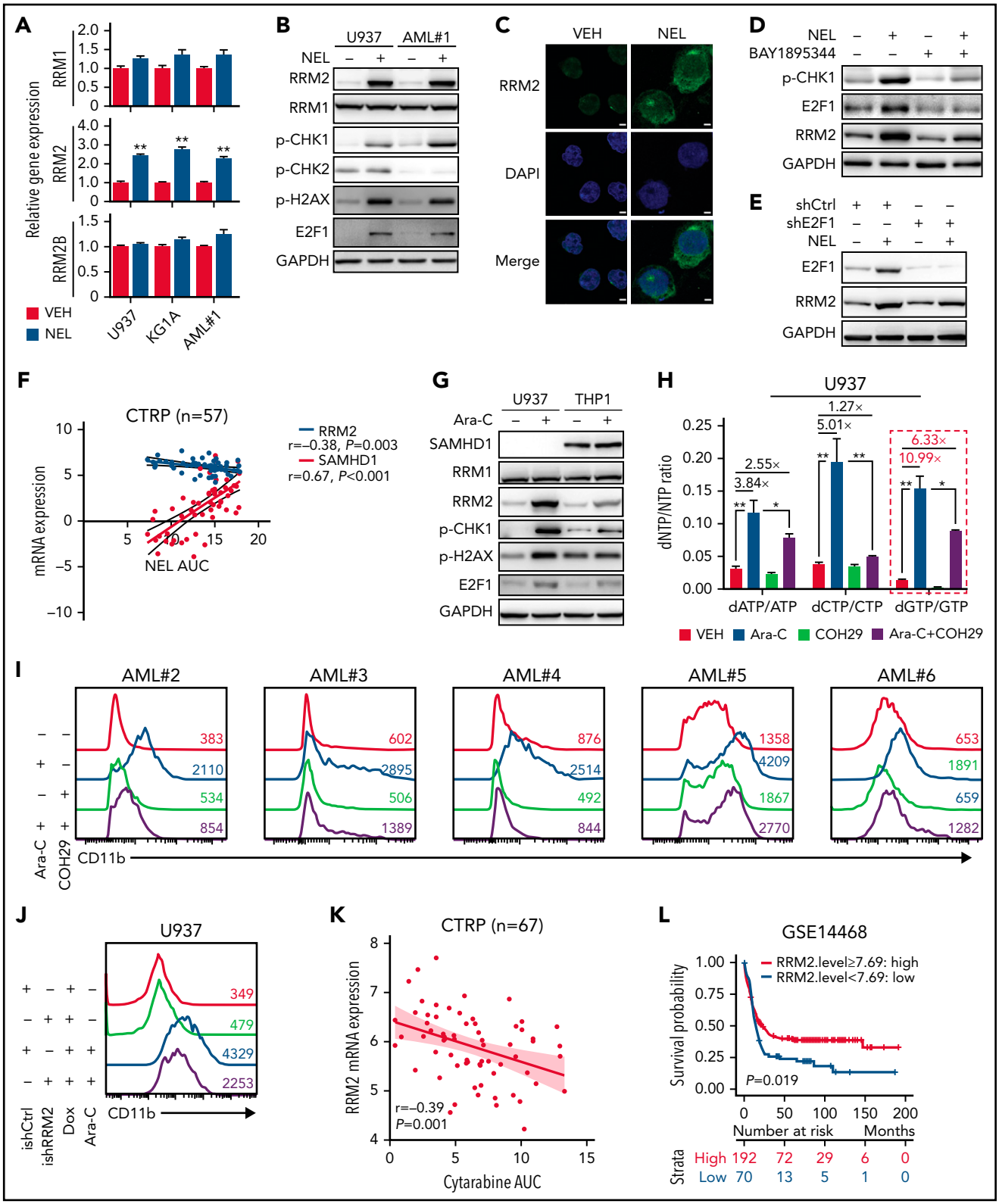

Figure 3. Replication stress signaling mediated RRM2 upregulation is responsible for myeloid differentiation. (A) Gene expression levels of RRM1, RRM2, and RRM2B were assessed by quantitative polymerase chain reaction analyses in indicated AML cells treated with vehicle or NEL for 12 hours (U937 and KG1A, 10 μM; AML#1, 20 μM). Data were first normalized to GAPDH levels and then vehicle-treated controls. Results represent mean ± SEM. $^{**}P < .01$. (B) Western blot of the indicated proteins in U937 and primary AML CD34$^+$ cells from specimen AML#1 treated with vehicle or NEL (U937, 10 μM; AML#1, 20 μM) for 12 hours. (C) Immunofluorescence analysis of RRM2 expression in U937 cells treated with vehicle or NEL (10 μM) for 12 hours. Scale bar, 5 μm. (D) Western blot of the indicated proteins in U937 cells treated with vehicle, NEL (10 μM), BAY1895344 (50 nM), or combination for 12 hours. (E) Western blot of the indicated proteins in U937 cells transduced with shRNA against *E2F1* (shE2F1) or scramble control (shCtrl) after NEL treatment (10 μM) for 12 hours. (F) Pearson correlation of RRM2 and SAMHD1 mRNA expression levels with NEL sensitivity in a panel of 57 hematopoietic cell lines. Data were sourced from Cancer Therapeutics Response Portal (CTRP). (G) Western blot of the indicated proteins in U937 and THP1 cells

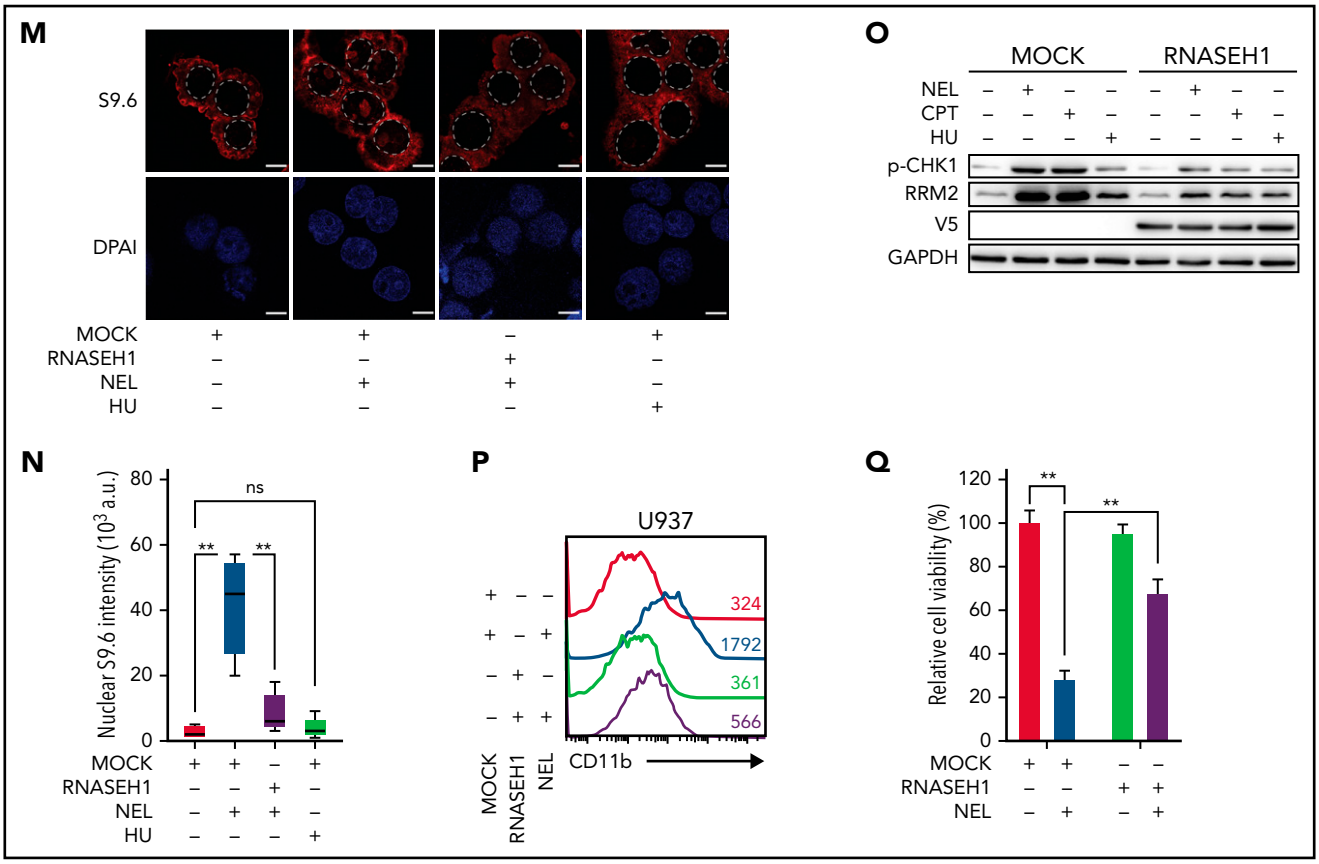

Figure 3 (continued) treated with vehicle or Ara-C (0.5 μM) for 12 hours. (H) U937 cells were treated with vehicle, Ara-C (0.5 μM), COH29 (10 μM), or combination for 12 hours, and intracellular dNTP levels were quantified relative to their NTP counterparts by HPLC/MS. Numbers denote the fold changes of dNTP/NTP ratios relative to vehicle-treated controls. Results represent mean ± SEM. $*P < .05$; $**P < .01$. (I) CD11b expression levels in primary AML CD34$^+$ cells (n = 5) treated with vehicle, Ara-C (0.5 μM), COH29 (10 μM), or combination for 96 hours. (J) CD11b expression levels of ishCtrl- and ishRRM2-U937 cells with or without Ara-C treatment (0.5 μM, 96 hours) after doxycycline induction. (K) Pearson correlation of RRM2 mRNA expression levels with Ara-C sensitivity in a panel of 67 hematopoietic cell lines. Data were sourced from CTRP portal. (L) Kaplan-Meier survival analysis of a cohort of patients with AML (GSE14468) after dichotomization for RRM2 mRNA levels below (blue, n = 70) and above (red, n = 192) 7.69 $\log_2$ transformed intensity ($P = .019$). (M-N) Representative immunofluorescence images (M) and quantification of nuclear S9.6 intensity (N) in U937 cells transduced with empty vector (MOCK) or V5-tagged RNASEH1 construct after treatment with NEL (10 μM) or HU (20 μM) for 6 hours. Regions of interest for specific quantification of nuclear S9.6 staining were highlighted by dotted white lines. Scale bar, 10 μm. Box-whisker plots indicate median, 25th to 75th percentile, and maximum and minimum values by line, box, and whiskers, respectively. ns, nonsignificant; $**P < .01$. (O) Western blot of the indicated proteins in MOCK- or RNASEH1-transduced U937 cells after treatment with vehicle, NEL (10 μM), CPT (20 nM), or HU (20 μM) for 12 hours. (P-Q) CD11b expression levels (P) and relative cell viability (Q) of MOCK- or RNASEH1-transduced U937 cells after treatment with vehicle or NEL (10 μM) for 96 hours. Results represent mean ± SEM. $**P < .01$.

cell viability as reported[18,47] (Figure 2I). dG treatment promoted a significant increase in total dGTP levels to an extent greater than that of any other dNTPs (Figure 2J; supplemental Figure 2R). Notably, addition of dC or dA could diminish dG's effects (Figure 2K; supplemental Figure 2R-S). Furthermore, addition of forodesine, an inhibitor of purine nucleoside phosphorylase,[48] could exacerbate dG-triggered imbalance, whereas forodesine alone was less effective than dG (supplemental Figure 2T). dG treatment induced differentiation and inhibited viability of AML cells within a clinically achievable dosage[49] (Figure 2L; supplemental Figure 2U-V). We further depleted *SAMHD1* as a safeguard of dNTP homeostasis[19] in SAMHD1-proficient THP1 cells (supplemental Figure 2W-Y) and observed enhanced dG-mediated differentiation and growth inhibition relative to *SAMHD1* wild-type (WT) controls (Figure 2M-N), confirming the importance of dNTP imbalance.

To evaluate the effects of dNTP pool imbalance on leukemia stem cell (LSC) activity, we conducted in vitro limiting dilution assay[50-52] using BM cells from *Mll-AF9* transgenic mice[53] or primary AML cells. dG treatment resulted in a decrease in LSC frequency and differentiation induction (Figure 2O; supplemental Figure 2Z). Relative to vehicle controls, dG pretreatment markedly decreased engraftment of leukemic cells in NSGS mice at 12 weeks after transplantation (Figure 2P-Q). Notably, secondary transplantation of BM cells from mice receiving dG-pretreated cells resulted in nearly complete elimination of leukemia engraftment (Figure 2R) compared with those of control cells, highlighting the impairment of LSC self-renewal (Figure 2S).

Replication stress-mediated RRM2 upregulation is responsible for myeloid differentiation

We next asked whether treatment of NEL, a known genotoxin, upregulated RNR subunits through DNA damage response machinery.[9,54] Among RNRs, RRM2 levels were significantly upregulated by NEL treatment (Figure 3A-B). Immunofluorescence revealed enhanced cytoplasmic level and nuclear localization of RRM2 (Figure 3C). Notably, NEL treatment for 12 hours

Table 1. Hazard rates for mRNA levels of RRM2 in AML patients treated with Ara-C

mRNA	GSE14468 cohort		TCGA cohort	
	Overall survival*	Overall survival†	Overall survival*	Overall survival†
RRM2	**0.68 (0.49-0.94; .02)**	**0.72 (0.51-1.01; .05)**	0.70 (0.43-1.15; .16)	0.81 (0.49-1.33; .40)

Shown are hazard rates, 95% confidence intervals, and *P* values calculated with Wald test. Bold text indicates $P < .05$.

*Data from univariate analysis.

†Data adjusted for age and sex.

significantly altered levels of *ATR* signaling effectors, including p-CHK1 and E2F1, whereas modest alterations were seen on p-CHK2 (Figure 3B). Consistently, unlike ATM inhibition, ATR inhibition or E2F1 knockdown reduced NEL-mediated upregulation of RRM2 (Figure 3D-E; supplemental Figure 3A-C), confirming that NEL treatment upregulated RRM2 via the ATR/CHK1/E2F1 axis.[55] RRM2 levels correlate with NEL sensitivity in hematopoietic cancer cell lines in contrast to the role of *SAMHD1* as reported[56] (Figure 3F; supplemental Figure 3D). Accordingly, NEL treatment caused more robust increased levels of RRM2 and DNA damage effectors in *SAMHD1* knockout (KO) THP1 cells compared with WT controls (supplemental Figure 3E), consistent with *SAMHD1*'s function in preventing Ara-GTP accumulation and decreasing replication stress.[21]

The mechanism of Ara-C action is similar to NEL[41,57]; thus, we asked whether differentiation induction seen after Ara-C treatment as reported previously[6,58] involved RRM2 activation. Indeed, Ara-C significantly increased RRM2, p-CHK1, E2F1, and dNTP levels in U937 cells but only induced modest changes in SAMHD1-proficient THP1 cells (Figure 3G; supplemental Figure 3F). Next, we assessed the role of RNR in Ara-C treatment effects by applying 2 strategies mentioned above. In 1, COH29 treatment alleviated dNTP imbalance (Figure 3H; supplemental Figure 3G) and weakened differentiation markers upregulation after Ara-C treatment (Figure 3I; supplemental Figure 3H-I). In another approach using ishRRM2-U937 as a model, Ara-C treatment resulted in less differentiation induction relative to that seen in ishCtrl-U937 cells (Figure 3J). Notably, RRM2 levels are strongly and positively correlated with Ara-C sensitivity (Figure 3K; supplemental Figure 3J), whereas *SAMHD1* is a resistant factor.[20,21] Additionally, we asked whether patients with AML exhibiting high RRM2 levels achieve better outcomes after treatment with Ara-C–based standard care. Indeed, we observed a positive correlation between higher RRM2 levels and longer overall survival (Figure 3L; supplemental Figure 3K-L; Table 1) through retrospectively analyzing both TCGA[59] and GSE14468[60] cohorts.

To further define the differentiation-related DNA insult by NEL treatment, we tested whether the insult associated with excessive formation of R-loops that specifically activate *ATR* signaling.[15,16,61] Interestingly, Ara-C is known to trigger R-loop formation,[62] likely because of transcription-replication conflicts. Similarly, NEL treatment enhanced R-loops formation evidenced by increased nuclear staining of the S9.6 antibody (Figure 3M-N). Overexpressing RNASEH1 to resolve R-loops remarkably abrogated ATR/CHK1 activation and RRM2 upregulation, thereby blocking differentiation induction and partially rescuing viability inhibition by NEL treatment (Figure 3M-Q). Moreover, HU did not induce R-loop formation (Figure 3M-N) or differentiation (supplemental Figure 3M), although it resulted in DNA damage as evidenced by CHK1 phosphorylation (Figure 3O).

We next asked whether non–DNA-incorporating compounds could induce differentiation in an RNR-dependent manner. Camptothecin (CPT), a topoisomerase I inhibitor, reportedly induces leukemia cell differentiation.[63] Similar to Ara-C, CPT treatment increased RRM2, p-CHK1, and E2F1 levels in AML cells (supplemental Figure 3N-O). Notably, the drug-induced effects on dNTP imbalance and differentiation were significantly rescued by RNR downregulation, whereas viability inhibition was partially reversed (supplemental Figure 3P-T). Moreover, CPT is also known to induce R-loop formation.[55] Consistently, overexpressing RNASEH1 abrogated ATR/CHK1 activation and RRM2 upregulation by CPT treatment (Figure 3O).

Genetically elevating RRM2 levels impairs AML maintenance

We asked whether direct upregulation of RRM2 would initiate differentiation. We first used THP1 as a model. Following CDK2-mediated phosphorylation of Thr33, WT RRM2 was recognized by Cyclin-F (CCNF) via the RxI motif (aa49-aa51) for degradation at G_2/M phase.[14] Although ectopic expression of WT FLAG-RRM2 marginally affected RRM2 levels, expression of RRM2 mutants exhibiting less binding affinity to CCNF[14] (RRM2-T33A [T33A] and RRM2-RxI/AxA [RxI/AxA]) promoted RRM2 accumulation (supplemental Figure 4A), thereby decreasing cell viability (supplemental Figure 4B). Given that RRM2 protein accumulated mostly after RxI/AxA overexpression (OE), we transduced an inducible RRM2-RxI/AxA mutant (iRxI/AxA) into THP1 for further analysis (Figure 4A; supplemental Figure 4C). After DOX induction, iRxI/AxA-transduced cells showed increased dNTPs, particularly a marked increase in dGTP, pronounced differentiation, and decreased viability relative to MOCK cells (Figure 4B-C; supplemental Figure 4D). To further enhance RRM2 activity, we exposed this inducible line to the combination of DOX plus NEL or DOX plus Ara-C. Relative to DOX alone, the combination further increased RRM2 levels, aggravated dNTP imbalance, enhanced CD11b induction, and inhibited viability (Figure 4A-C; supplemental Figure 4D). To assess outcomes in vivo, we transplanted these engineered cells into NSGS mice and treated mice with combination of DOX plus NEL or DOX plus phosphate-buffered saline (PBS). Mice injected with MOCK cells receiving combination of DOX plus PBS succumbed to systemic disease shortly, whereas mice injected with iRxI/AxA cells receiving combination of DOX plus PBS survived significantly longer and exhibited reduced leukemic burden (Figure 4D-E). Relative to PBS controls, NEL treatment further decreased leukemic burden and prolonged survival in mice engrafted with iRxI/AxA cells

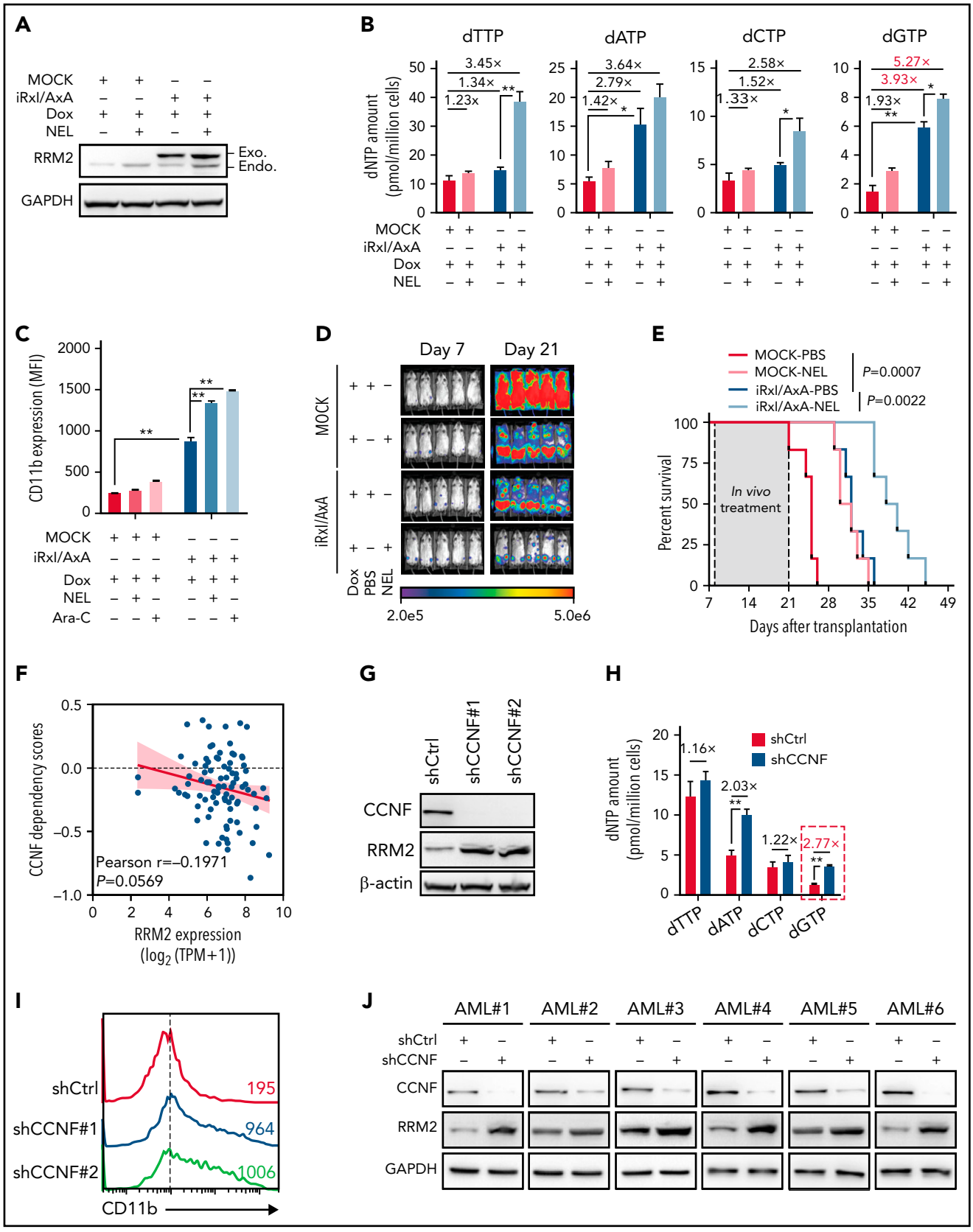

Figure 4. Genetically elevating RRM2 levels impairs AML maintenance. (A-B) Western blot of RRM2 protein levels (A) and primer extension assay of intracellular dNTP levels (B) in THP1 cells engineered with empty vector (MOCK) or inducible RRM2 RxI/AxA (iRxl/AxA) mutant, further treated with vehicle or NEL (20 μM, 12 hours) after doxycycline (DOX) induction. RxI/AxA, CCNF binding-deficient RRM2 construct: RxI motif located at RRM2 residues aa49-aa51, reportedly binding to cyclin F, was mutated to AxA. Numbers denote the fold changes relative to vehicle-treated MOCK controls. For panel B, results represent mean ± SEM. *$P < .05$; **$P < .01$. (C) CD11b expression levels in MOCK- or iRxl/AxA-THP1 cells treated with vehicle, NEL (20 μM), or Ara-C (0.5 μM) for 96 hours after DOX induction. Results represent

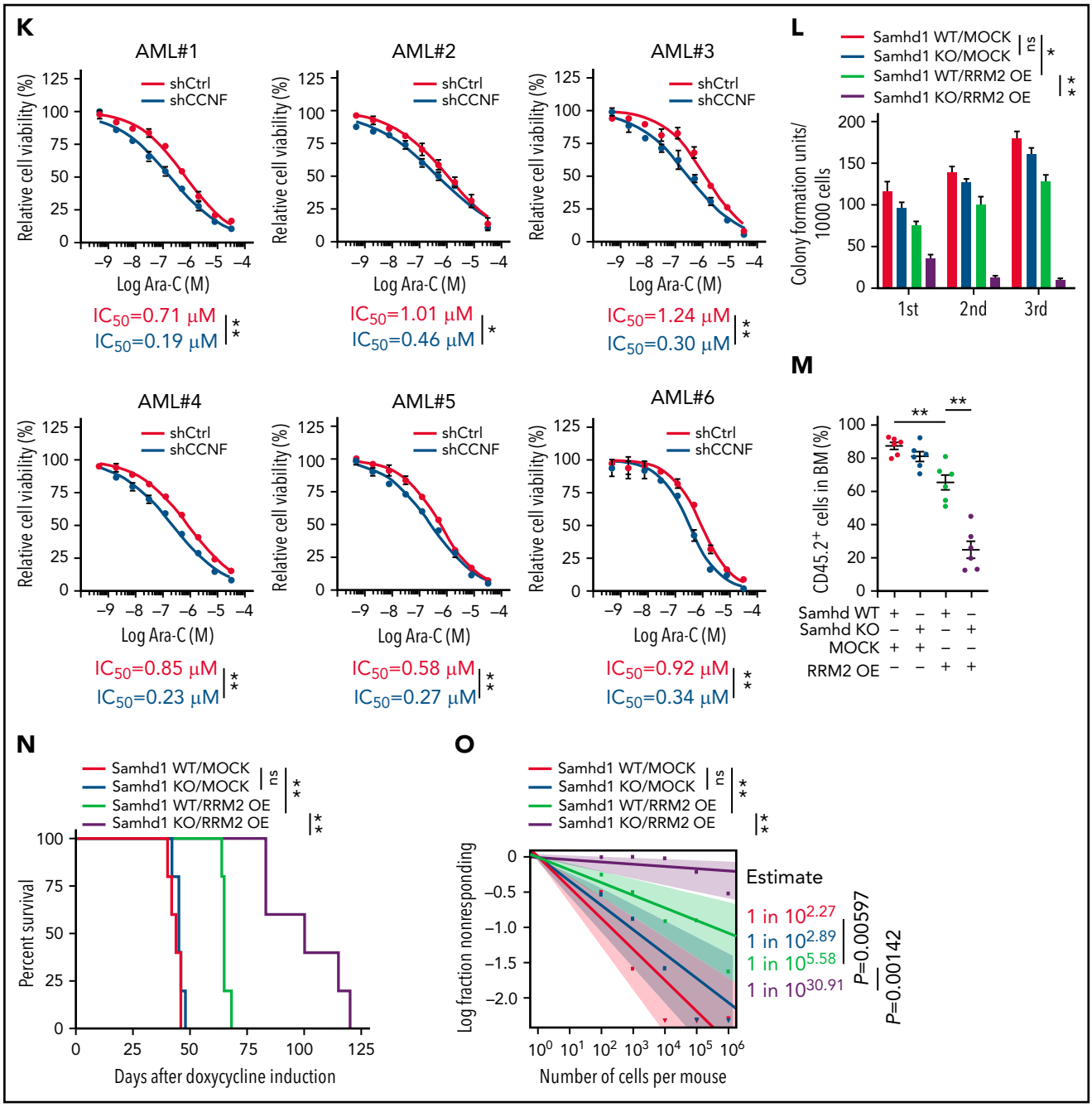

Figure 4 (continued) mean ± SEM. $^{**}P < .01$. (D-E) Engineered THP1 cells (1×10^6 cells per mouse) were injected into NSGS mice. Following engraftment, 2 groups of mice receiving either MOCK cells or iRxl/AxA cells were treated with DOX (10 mg/kg, daily). In MOCK or iRxl/AxA transplants, mice were divided into 2 treatment groups injected with either vehicle (PBS) or NEL (217 mg/kg, IV daily; n = 5 per group) and then assessed for engraftment by bioluminescence imaging (D) or monitored for survival (E). (F) Pearson correlation of RRM2 mRNA expression with *CCNF* gene dependency scores in 94 hematologic cancer cell lines, sourced from Depmap portal. The *x* axis denotes to RRM2 expression levels of cell lines presented as log2-transformed TPM values. (G) Western blot of the indicated proteins in THP1 cells transduced with lentiviral vectors expressing shRNA against *CCNF* (shCCNF#1 [chosen to be used further, namely shCCNF], shCCNF#2) or scramble control (shCtrl), followed by G_2/M enrichment through treatment with nocodazole (100 ng/mL, 16 hours). (H) Intracellular dNTP levels of shCtrl- or shCCNF-THP1 cells followed by G_2/M enrichment through treatment with nocodazole (100 ng/mL, 16 hours). Numbers denote the fold changes relative to shCtrl-THP1 cells. Results represent mean ± SEM. $^{**}P < .01$. (I) CD11b expression levels in THP1 cells transduced with shCtrl, shCCNF#1, or shCCNF#2 lentivirus for 4 days. (J) Western blot of the indicated proteins in primary AML CD34$^+$ cells (n = 6) transduced with shCtrl or shCCNF lentivirus, followed by G_2/M enrichment through treatment with nocodazole (100 ng/mL, 16 hours). (K) Primary AML CD34$^+$ cells (n = 6) were transduced with shCtrl or shCCNF lentivirus before viability inhibition assay for 96 hours in the presence of Ara-C at the indicated concentrations. The IC_{50} values between cells transduced with shCtrl lentivirus and their shCCNF counterparts were analyzed by means of extra-sum-of-squares *F* test. Results represent mean ± SEM. $^{*}P < .05$; $^{**}P < .01$. (L) Serial replating of *Samhd1* WT/MOCK, *Samhd1* KO/MOCK, *Samhd1* WT/*RRM2* OE, and *Samhd1* KO/*RRM2* OE cells engineered from *MA9*$^+$ murine AML cells. Results represent mean ± SEM. ns, nonsignificant; $^{*}P < .05$; $^{**}P < .01$. (M) Percentages of CD45.2$^+$ donor chimerism in BM of recipients (n = 6 per group) transplanted with engineered cells as indicated on day 30 after DOX induction. Results represent mean ± SEM. $^{**}P < .01$. (N) Survival of CD45.1$^+$ congenic recipients transplanted with engineered *MA9*$^+$ murine AML cells as indicated. Doxycycline induction (10 mg/kg, daily) started 2 weeks after transplantation. (O) In vivo LDA assay showing LSC frequency changes in *MA9*$^+$ primary murine AML cells after *Samhd1* KO or *RRM2* OE.

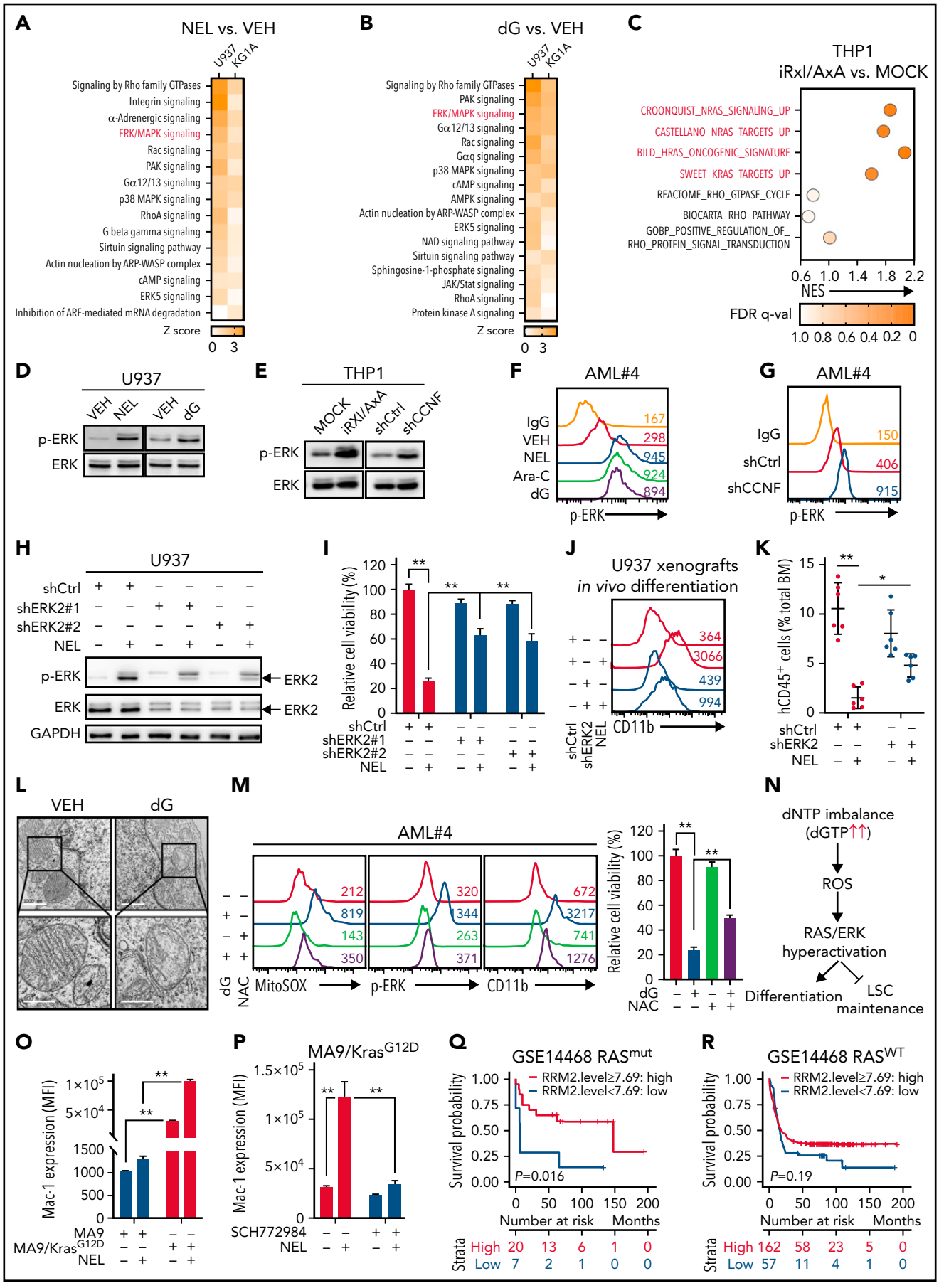

Figure 5.

(Figure 4D-E). Similar results were seen in leukemic mice treated with Ara-C (supplemental Figure 4E-F).

To assess effects of stimulating RRM2 activity in primary AML cells, we used a strategy of *CCNF* depletion.[14] We noted *CCNF* dependency score was negatively correlated with RRM2 basal levels in 94 hematologic cancer cell lines (Figure 4F). Indeed, *CCNF* knockdown (KD) in THP1 cells promoted RRM2 accumulation, created dNTP imbalance, induced differentiation, and decreased cell growth (Figure 4G-I; supplemental Figure 4G). To determine whether *RRM2* was required for *CCNF* KD effects, we established an *RRM2*-low THP1 line as described above. After DOX treatment, ishRRM2-THP1 cells exhibited decreased RRM2 levels (supplemental Figure 4D). *CCNF* KD significantly increased RRM2 and CD11b in ishCtrl-THP1 cells, whereas it only marginally increased RRM2 in ishRRM2-THP1 cells, with no change in CD11b levels (supplemental Figure 4H-I), suggesting that *CCNF* KD effects were mainly dependent on RRM2. Next, we depleted *CCNF* in primary AML cells and observed varying increases in RRM2 levels among specimens (n = 6; Figure 4J), hinting additional RRM2 regulatory mechanisms other than CCNF.[64,65] We further assessed effects of combining *CCNF* KD with Ara-C or NEL treatment. *CCNF* KD decreased the half-maximal inhibitory concentration (IC_{50}) values of both drugs (Figure 4K; supplemental Figure 4J) and enhanced NEL-induced differentiation compared with NEL alone at a fixed dose (20 μM; supplemental Figure 4K).

We asked whether aggravating dNTP imbalance by deleting *SAMHD1* could enhance RRM2 hyperactivation mediated inhibitory effects. To do so, we used *Mll-AF9*/*Samhd1* KO mice (Samhd1-KO) generated through crossing *Samhd1* KO mice[23] to *Mll-AF9* transgenic mice. We expressed iRxI/AxA construct or MOCK control in *Samhd1*-KO or *Samhd1*-WT BM cells, respectively, resulting in 4 groups: *Samhd1*-WT/MOCK, *Samhd1*-KO/MOCK, *Samhd1*-WT/*RRM2* OE, and *Samhd1*-KO/*RRM2* OE. We then used these engineered cells for CFC re-plating. Interestingly, murine AML cells harboring iRxI/AxA showed significantly decreased CFC compared with MOCK cells in primary and serial re-platings; whereas *Samhd1* KO alone barely affected CFC, it further compromised CFC in AML cells harboring iRxI/AxA (Figure 4L). To test the hypothesis in vivo, we transplanted engineered cells into CD45.1-expressing congenic recipient mice for leukemia assessment. iRxI/AxA-expressing *MA9* leukemic mice exhibited reduced leukemic chimerism in BM and improved survival relative to MOCK controls (Figure 4M-N). Notably, BM cells from iRxI/AxA-expressing *MA9* leukemic mice exhibited RRM2 overexpression and dGTP overproduction (supplemental Figure 4L-M). Moreover, *Samhd1* KO combined with iRxI/AxA expression further decreased engraftment and extended leukemic mice survival compared with iRxI/AxA expression alone (Figure 4M-N). To test whether genetically elevating RRM2 alone or in combination with *Samhd1* KO affected LSC activity, we conducted in vivo limiting dilution assays by establishing murine AML transplants using those engineered cells.[52] Similarly, iRxI/AxA expression alone resulted in a remarkable decrease in LSC frequency, and the combination of *Samhd1* KO and iRxI/AxA expression effectively inhibited in vivo repopulating capacity of AML cells (Figure 4O).

ERK activation contributes to myeloid differentiation

To define downstream pathway that conferred outcomes of dNTP imbalance, we assessed gene expression profiles in NEL or dG-treated AML cell lines (U937 and KG1A) by RNA-seq analyses (supplemental Tables 8-11). Ingenuity pathway analysis revealed Rho family GTPase signaling and ERK/MAPK signaling as top upregulated pathways in both treatments (Figure 5A-B). To validate whether these 2 pathways were effectors of RRM2 hyperactivation, we performed RNA-seq analyses of iRxI/AxA- and MOCK-THP1 cells after DOX treatment (supplemental Table 12). Gene set enrichment analysis revealed significant enrichment of RAS/ERK pathway signatures in iRxI/AxA-THP1 cells (Figure 5C), suggesting the role of *ERK* signaling as downstream of RRM2 hyperactivation. We further confirmed ERK activation after NEL, dG, or Ara-C treatment in AML cells (Figure 5D,F; supplemental Figure 5A). Of note, either iRxI/AxA OE or *CCNF* KD resulted in increased phospho-ERK in THP1 or primary AML specimens, respectively (Figure 5E,G; supplemental Figure 5B). To address the biological relevance of ERK activation, we established a U937 line with low basal *ERK* signaling using *ERK2* shRNA. Although *ERK2* knockdown slightly decreased cell

Figure 5. ERK activation contributes to myeloid differentiation. (A-B) U937 or KG1A cells treated with or without NEL (10 μM, 24 hours) (A), with or without dG (10 μM, 24 hours) (B), were collected for RNA-seq analysis. Upregulated intracellular signaling pathways based on ingenuity pathway analysis (Z score > 0) were shown in both cell lines. ERK/MAPK pathway is highlighted in red. (C) Scattergrams of RAS GTPase-related gene sets (red) and Rho GTPase-related gene sets (black) based on enrichment analyses of differentially expressed genes in MOCK- and iRxI/AxA-THP1 cells after doxycycline induction. The color indicates the false discovery rate *q* values. NES, normalized enrichment score. (D) Western blot of phospho-ERK and total ERK levels in U937 cells treated with vehicle, NEL (10 μM) or dG (10 μM) for 24 hours. (E) Western blot of phospho-ERK and total ERK levels in MOCK- and iRxI/AxA-THP1 cells after doxycycline induction (i) and THP1 cells transduced with shCtrl or shCCNF lentivirus (ii). (F) Phospho-ERK levels in primary AML $CD34^+$ cells from specimen AML#4 treated with vehicle, NEL (20 μM), Ara-C (0.5 μM), or dG (15 μM) for 24 hours. (G) Phospho-ERK levels in primary AML $CD34^+$ cells from specimen AML#4 transduced with shCtrl or shCCNF lentivirus. (H) Western blot of the indicated proteins in U937 cells transduced with lentiviral vectors expressing shRNA against *ERK2* (shERK2#1, shERK2#2 [chosen to be used further, namely shERK2]) or scramble control (shCtrl), followed by treatment with NEL (10 μM) for 24 hours. (I) Relative cell viability of U937 cells transduced with shCtrl, shERK2#1, or shERK2#2 lentivirus followed by treatment with NEL (10 μM) for 96 hours. Results represent mean ± SEM. $^{**}P < .01$. (J-K) Representative CD11b expression (J) and percentages (K) of human $CD45^+$ cells in BM of recipients (n = 6 per group) transplanted with shCtrl- or shERK2-U937 cells, followed by in vivo administration with vehicle (PBS) or NEL (217 mg/kg, IV, daily) for 7 days. For panel J, data from 1 representative mouse in each group are shown. For panel K, results represent mean ± SEM. $^{*}P < .05$; $^{**}P < .01$. (L) Transmission electron microscopy images of mitochondrial cristae in U937 cells treated with vehicle or dG (10 μM) for 24 hours. Scale bar, 1 μm (i) or 0.5 μm (ii). (M) Mitochondrial superoxide levels, phospho-ERK levels, CD11b expression levels, and relative cell viability of primary AML $CD34^+$ cells from specimen AML#4 treated with vehicle, dG (15 μM), NAC (2 mM), or combination. Mitochondrial superoxide and phospho-ERK analyses were performed after treatment for 24 hours. CD11b expression and cell viability analyses were performed after treatment for 96 hours. For cell viability, results represent mean ± SEM. $^{**}P < .01$. (N) A schematic diagram demonstrating the casual relationships among dNTP imbalance, mitochondrial ROS release, RAS/ERK hyperactivation, and differentiation/LSC maintenance. (O) Mac-1 expression levels in murine $MA9^+$ and $MA9/Kras^{G12D}$ cells treated with vehicle or NEL (20 μM) for 96 hours. Results represent mean ± SEM. $^{**}P < .01$. (P) Mac-1 expression levels in murine $MA9/Kras^{G12D}$ cells pretreated with SCH772984 (2 μM) for 6 hours, followed by treatment with NEL (20 μM) for 96 hours. Results represent mean ± SEM. $^{**}P < .01$. (Q) Kaplan-Meier survival analysis of a cohort of patients with AML (GSE14468) carrying *RAS* mutations after dichotomization for RRM2 mRNA levels below (blue, n = 7) and above (red, n = 20) 7.69 log_2-transformed intensity ($P = .016$). (R) Kaplan-Meier survival analysis of a cohort of patients with AML (GSE14468) carrying WT-*RAS* after dichotomization for RRM2 mRNA levels below (blue, n = 57) and above (red, n = 162) 7.69 log_2-transformed intensity ($P = .19$).

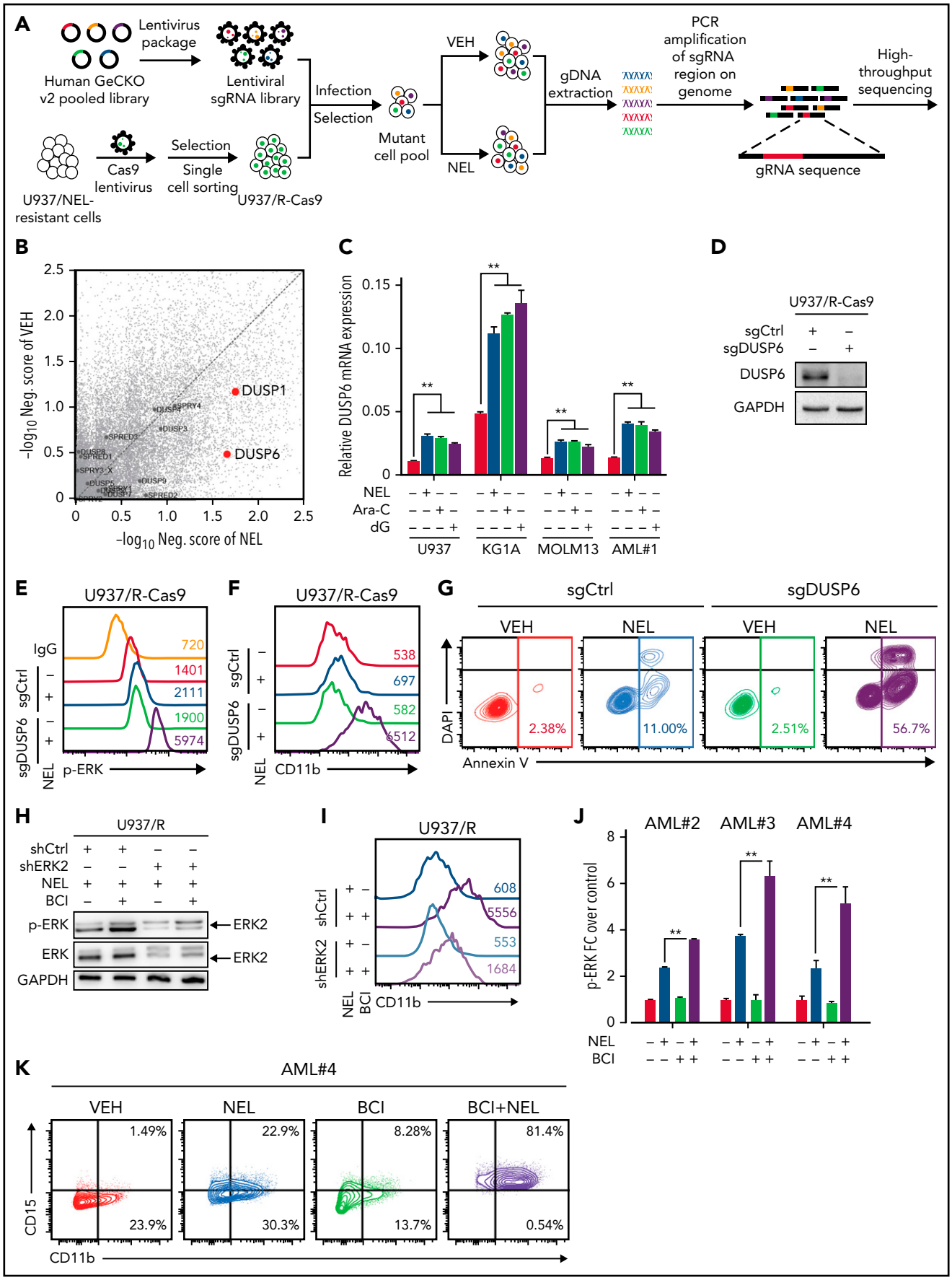

Figure 6. Loss-of-function screen identified synthetic lethal interaction between DUSP6-KO and nelarabine treatment. (A-B) Experimental design of genome-wide CRISPR/Cas9 screen for synthetic lethal partner of NEL treatment in NEL-resistant subline U937/R (A). Briefly, *Cas9* expressing-U937/R cells were transduced with GeCKO gRNA library. After culturing for 7 days, cells were divided into 2 groups for treatment with vehicle or NEL (20 μM). After another 7 days of exposure, sgRNA

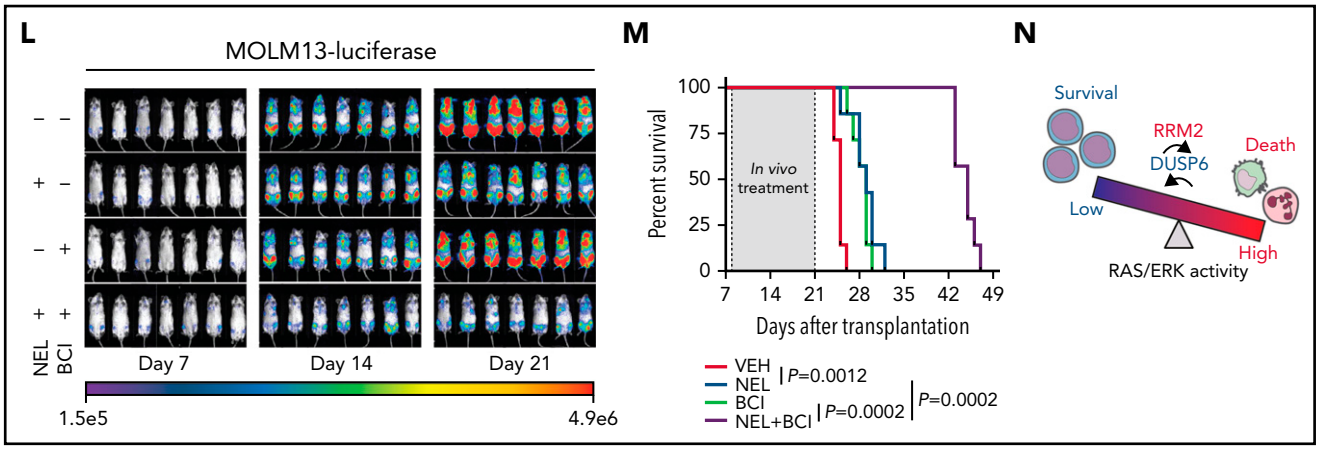

Figure 6 (continued) representation was assessed by sequencing. The gene negative scores (B) were calculated using MAGeCK-MLE module. Reported ERK negative feedback regulators were labeled. The red dots represent preferential depletion of *DUSP1* and *DUSP6* sgRNAs following NEL treatment over vehicle control. (C) Relative DUSP6 expression levels in indicated AML cells treated with vehicle, NEL (10 μM for U937 and KG1A, 20 μM for MOLM13 and AML#1), Ara-C (0.5 μM), or dG (10 μM for U937 and KG1A, 15 μM for MOLM13 and AML#1) for 24 hours. Results represent mean ± SEM. $^{**}P < .01$. (D) Western blot of DUSP6 proteins in U937/R-Cas9 cells transduced with lentiviral vectors expressing sgRNA against *DUSP6* (sgDUSP6) or nontargeting control (sgCtrl). (E) Phospho-ERK levels in sgCtrl- or sgDUSP6-U937/R cells treated with vehicle or NEL (20 μM) for 24 hours. (F-G) CD11b expression levels (F) and apoptosis (G) of sgCtrl- or sgDUSP6-U937/R cells treated with vehicle or NEL (20 μM) for 96 hours. (H) Western blot of the indicated proteins in U937/R cells transduced with lentiviral vectors expressing shRNA against *ERK2* (shERK2) or scramble control (shCtrl), followed by treatment with NEL (20 μM) alone or NEL (20 μM) plus BCI (1 μM) for 24 hours. (I) CD11b expression levels in shCtrl- or shERK2-U937/R cells treated with NEL (20 μM) alone or NEL (20 μM) plus BCI (1 μM) for 96 hours. (J) Relative phospho-ERK levels in primary AML $CD34^+$ cells (n = 3) treated with vehicle, NEL (20 μM), BCI (1 μM), or combination for 24 hours. Data were normalized to vehicle-treated controls. Results represent mean ± SEM. $^{**}P < .01$. (K) CD11b and CD15 expression levels in primary AML $CD34^+$ cells from specimen AML#4 treated with vehicle, NEL (20 μM), BCI (1 μM), or a combination for 96 hours. (L-M) MOLM13-luciferase cells (1×10^6 cells per mouse) were injected into sublethally irradiated NSGS mice. Following engraftment, mice were treated with vehicle (PBS), NEL (217 mg/kg, IV, daily), BCI (10 mg/kg, intraperitoneally, daily), or a combination for 2 weeks (n = 7 per group), assessed for engraftment by in vivo bioluminescence imaging (L) and monitored for survival (M). (N) A schematic model showing that the response to RRM2 hyperactivation-mediated dNTP imbalance depends on reaching a lethal threshold of RAS/ERK activity, and *DUSP6* activity may antagonize this lethal effect.

growth relative to controls, it blocked NEL-induced growth inhibition effects (Figure 5H-I). We further injected U937 cells expressing either *ERK2* shRNA or nontargeting control into NSGS mice and treated both groups with NEL. Relative to mice receiving *ERK2*-intact AML cells, mice receiving *ERK2* KD cells showed less therapeutic responses following NEL treatment (Figure 5J-K). Moreover, pretreatment with ERK inhibitors to downregulate its basal signaling partially rescued the effects of NEL or dG treatment (supplemental Figure 5C-F), whereas long-term treatment of an ERK or MEK inhibitor alone eliminated AML CFC (supplemental Figure 5G), likely because of complete abrogation of *ERK* signaling.[66,67]

Severe dNTP imbalance reportedly impairs mitochondrial DNA replication,[68,69] resulting in mitochondrial stress and release of reactive oxygen species (ROS), which leads to ERK activation.[70] Accordingly, dG or NEL treatment caused disruption of mitochondrial matrix morphology and loss of mitochondrial cristae (Figure 5L; supplemental Figure 5H). Moreover, dG treatment increased mitochondrial superoxide, decreased mitochondrial membrane potential, and induced leakage of mitochondrial DNA into cytoplasm (Figure 5M; supplemental Figure 5I-K). Notably, addition of ROS scavenger *N*-acetyl cysteine (NAC) reversed mitochondria superoxide increase, dampened ERK activation, and partially rescued cellular outcome by dG treatment in AML cells (Figure 5M; supplemental Figure 5K-L), indicating that mitochondrial ROS release links dNTP imbalance to ERK activation (Figure 5N). Moreover, $CD34^+CD38^-$ AML cells showed increased differentiation and reduced CFC after dG treatment, whereas these effects were partially rescued by NAC treatment (supplemental Figure 5M-N), suggesting that both differentiation and LSC impairment are downstream of mitochondrial dysfunction (Figure 5N).

Hyperactive RAS reportedly promotes commitment of differentiation through ERK hyperactivation.[71-74] To determine whether oncogenic *RAS* cooperated with NEL-induced ERK activation to induce differentiation and growth inhibition, we used splenocytes from mice bearing conditional oncogenic *Kras* ($Kras^{Lox\text{-}Stop\text{-}Lox\ (LSL)\ G12D/+}$/$Vav\text{-}Cre^+$),[75,76] followed by *Mll-AF9* transduction. Relative to $Vav\text{-}Cre^+$ splenocytes transformed by *MA9* alone, *MA9*/$Kras^{G12D}$ doubly transformed cells were more vulnerable to NEL-induced inhibitory effects (Figure 5O; supplemental Figure 5O). Notably, ERK inhibition partially rescued NEL's effects on *MA9*/$Kras^{G12D}$ cells (Figure 5P; supplemental Figure 5P). We next asked whether RRM2 level predicted prognosis in patients carrying oncogenic *RAS* after Ara-C treatment, which also primed *ERK* signaling (Figure 5F; supplemental Figure 5A). To do so, we reanalyzed clinical outcomes of *RAS* mutant or *RAS* WT cases from the GSE14468 cohort containing sufficient *RAS* mutant cases.[60] Indeed, high RRM2 level predicted longer survival for AML patients carrying *RAS* mutations, whereas in patients with WT *RAS*, RRM2 level was less predictive (Figure 5Q-R; supplemental Table 13).

Loss-of-function screen identified synthetic lethal interaction between DUSP6-KO and nelarabine treatment

Drug combination is desired to achieve maximal efficacy. To identify NEL-based combination therapy, we performed a genome-wide clustered regularly interspaced short palindromic repeats (CRISPR) screen in a U937 subline resistant to NEL

(U937/R; Figure 6A). This subline (IC_{50} = 42.3 μM) was generated by gradual adaptation of parental cells (IC_{50} = 3.8 μM) to 50 μM NEL over months.[77] After *Cas9*$^{+}$ clonal derivation (supplemental Figure 6A), we transduced cells with GeCKO guide RNA (gRNA) library[78] and treated with 20 μM NEL for 7 days to negatively enrich candidate gRNAs associated with drug response.[79] Among the top hits, we identified *NT5C2* to be significantly depleted in NEL-treated cells (supplemental Table 14), which encodes a nucleotidase reportedly to inactivate the active metabolites of purine analogs.[80-83] Herein, given that NEL's effects associated with ERK activation, and hyperactivation of ERK can be deleterious to cancer cells,[84,85] we thus analyzed gRNAs targeting genes encoding those negative feedback regulators of *ERK* signaling[84,85] (Figure 6B), including the dual-specificity phosphatases (*DUSPs*), the sprouty proteins, and the sprouty-related EVH1 domain-containing proteins.[84,86] Among those genes, *DUSP1* and *DUSP6* were markedly depleted in NEL-treated vs vehicle-treated cells[87] (Figure 6B; supplemental Table 14). Four of 6 gRNAs targeting *DUSP6* were depleted in NEL-treated cells (supplemental Figure 6B). Given its higher abundancy than DUSP1 (supplemental Figure 6C) and its adaptive upregulation after short exposure to drug treatment (Figure 6C), we prioritized *DUSP6* for further investigation.

In U937/R cells, *DUSP6* depletion potentiated NEL-induced ERK activation, differentiation, and apoptosis than did comparably treated *DUSP6* WT cells (Figure 6D-G). To determine whether targeting *DUSP6* would enhance NEL's effects, we tested a small molecule inhibitor of DUSP6, 2-benzylidene-3-(cyclohexylamino)-1-Indanone hydrochloride (BCI).[88] Analogously, the addition of BCI re-sensitized U937/R cells to NEL-induced ERK activation, differentiation, and apoptosis (supplemental Figure 6D-F), whereas those effects were partially blocked by *ERK2* knockdown (Figure 6H-I; supplemental Figure 6G). Enhanced leukemia targeting effects by combination were also seen in primary AML cells (Figure 6J-K; supplemental Figure 6H). To assess outcomes in vivo, we used NSGS models xenografted with MOLM13 cells, because its sensitivity to NEL was comparable to those of most primary AML specimens (supplemental Figure 6I). Although NEL treatment alone had modest effects, the combination significantly alleviated leukemia burden (Figure 6L-M; supplemental Figure 6I), with a comparable survival benefit to that of standard chemotherapy (supplemental Figure 6K), suggesting the response to NEL depends on reaching a lethal threshold of ERK activity, and *DUSP6* may antagonize that effect (Figure 6N).

Discussion

Our results highlight the importance of dNTP homeostasis in myeloid differentiation. We show that dNTP imbalance caused by RRM2 hyperactivation through either drug treatment or genetic manipulation overcomes the differentiation blockade. Specifically, dGTP level is most vulnerable to be perturbated. Accordingly, dG is most potent in inducing differentiation and LSC ablation among all dNs. We also note that *SAMHD1* may underlie varying responses to dG treatment in AML cells; *SAMHD1* KO in AML cells remarkably enhances dG or *RRM2* OE-induced differentiation and self-renewal ablation (Figures 2M-N and 4L-O). Therefore, *SAMHD1* may counteract dNTP pool changes initiated by drug treatment or RRM2 upregulation, lessening the cellular outcome.

Our study reveals a novel role of *RRM2* in promoting AML differentiation. Specifically, treatment of NEL, Ara-C, or CPT induces RRM2 hyperactivation, in agreement with previous reports of increases in RNR subunit levels after replication stress.[55] In particular, this drug-induced RNR activation leads to imbalanced dNTPs, in contrast with dNTP changes after allosteric RNR activation during cell cycling.[42] One explanation for this discrepancy in dNTP outcomes could be the duration of RRM2 upregulation, which may determine the extent of RNR activation. Moreover, SAMHD1 determines the extent to which RNR is activated, given its restriction on Ara-CTP or Ara-GTP accumulation.[89] Nevertheless, in SAMHD1-proficient AML cells, overexpression of a stable RRM2 mutant promotes tumor regression and impairs LSC self-renewal (Figure 4).

We identify augmented R-loop formation underlies differentiation induction by NEL treatment. R-loops specifically activate *ATR* signaling as previously reported.[15,16] Consistently, both Ara-C[62] and CPT[90] reportedly trigger R-loop formation,[91] whereas HU does not.[16] These results highlight the role of R-loop–initiated DNA damage in promoting differentiation, whereas we do not exclude the possibility that other actions of these genotoxins (NEL, Ara-C) also serve as mechanisms of lethality (eg, incorporation into nascent DNA).

ERK is an important player in controlling hematopoietic cell activity.[92] Complete repression of *ERK* signaling by MEK or ERK inhibitors causes lethality,[66,67] whereas excessive ERK activation also compromises viability of cancer cells.[84,85,93] Accordingly, our data extend the emerging concept that hyperactivation of ERK can be deleterious in the context of AML. Notably, *RAS* mutations predict a better therapeutic response in patients with AML treated with high-dose cytarabine[74,94] but show resistance to a venetoclax-based regimen.[72] Moreover, we provide a therapeutic strategy to further enhance *ERK* signaling in AML cells primed by NEL treatment through cotargeting *DUSP6*, thereby surpassing an ERK hyperactivation-related lethal threshold (Figure 6). The combination of BCI and NEL not only suppresses leukemogenesis in an AML xenograft model but exhibits better tolerability than standard chemotherapy (supplemental Figure 6J-L).

In conclusion, we show that disrupting dNTP pool homeostasis overcomes differentiation blockade of AML cells and impairs LSC self-renewal. Our study prompts a reappraisal of therapeutic response in patients with *RAS*-mutated AML with considerations of factors controlling dNTP homeostasis, such as *RRM2* and *SAMHD1*. Finally, we provide a rationale for further evaluation of the combination of nelarabine with a DUSP6 inhibitor against AML.

Acknowledgments

The authors thank COH Comprehensive Cancer Center, as well as patients, donors, and their physicians for providing primary specimens for this study, Jianjun Chen for providing Cas9-expressing THP1 cells, Jan Rehwinkel at University of Oxford for constitutive Samhd1 KO mice, Dong-er Zhang at University of California, San Diego, for RNASEH1 vectors, Johanna Ten Hoeve at UCLA metabolomics center for assistance with metabolites measurements, and Stemcyte Inc. for the cord blood (CB) sample. The authors also thank Elise Lamar and Marjorie Robbin for help in manuscript editing and proofreading.

This work was supported in part by National Institutes of Health (NIH) grant R01 CA152108 and Department of Defense impact award CA190124 to J.Z., NIH grant R01 CA2062101 and Cancer Prevention & Research Institute of Texas grant DP150061 to S.T., and Gehr Family Center for Leukemia Research support to L.L. The authors acknowledge the support of the Animal Resources Center, Analytical Cytometry Core, Bioinformatics, Light Microscopy, Electron Microscopy, Integrative Genomics Core, Mass Spectrometry & Proteomic Core at COH Comprehensive Cancer Center, supported by the NIH, National Cancer Institute under award P30CA33572.

The content is solely the responsibility of the authors and does not necessarily represent official views of the NIH.

Authorship

Contribution: H.W. designed and performed experiments, interpreted results, and wrote the manuscript; X.H. designed and performed experiments including bioinformatic data mining, primer extension assay for dNTP measurements, immunofluorescence, and CRISPR-Cas9 screen, and reviewed the manuscript; Lei Zhang performed Western blot analyses and reviewed the manuscript; H.D. assisted with animal experiments and reviewed the manuscript; F.H. performed the CFC assay, *Mll-AF9* retrovirus packaging and transduction, and animal experiments; J.X. performed flow cytometry analysis; M.L. performed statistical analyses; W.C. performed transcriptomic analyses; X.L. and K.V.P. performed quantitative MS analyses; W.H. assisted with flow cytometry analyses and animal experiments; Z.L. and Lianjun Zhang assisted with experiments; L.X.T.N. performed transmission electron microscopy experiments; L.Y. interpreted CRISPR screen results; L.F. reviewed RNA-seq results; D.J.G. provided ishRRM2/iRRM2-T33A constructs; J.Z. provided murine $Kras^{G12D/+}$ splenocytes; A.S. provided AML samples; D.H. provided compound COH29; D.B.S. provided ER-HoxA9 cells; P.P., C.-W.C., Y.-H.K., G.M., S.T., H.J., and X.W. reviewed and edited the manuscript; and L.L. designed the study, interpreted data, and prepared the manuscript with input from others.

Conflict-of-interest disclosure: D.B.S. is a cofounder and holds equity in Clear Creek Bio, is a consultant and holds equity in SAFI Biosolutions, and is a consultant for Keros Therapeutics. The remaining authors declare no competing financial interests.

ORCID profiles: P.P., 0000-0003-1360-6039; C-W.C., 0000-0002-8737-6830; Y-H.K., 0000-0003-2595-0419; S.T., 0000-0002-7230-0307.

Correspondence: Ling Li, Department of Hematological Malignancies Translational Science, Gehr Family Center for Leukemia Research, Hematologic Malignancies and Stem Cell Transplantation Institute, Beckman Research Institute of City of Hope, Monrovia Research Center 2005, 1500 E. Duarte Rd, Duarte, CA 91010; e-mail: lingli@coh.org; Hongchuan Jin, Laboratory of Cancer Biology, Provincial Key Laboratory of Biotherapy in Zhejiang, Sir Run Run Shaw Hospital, Zhejiang University, 3 East Qingchun Rd, Hangzhou 310016, China; e-mail: jinhc@zju.edu.cn; and Xian Wang, Department of Medical Oncology, Sir Run Run Shaw Hospital, Zhejiang University, 3 East Qingchun Rd, Hangzhou 310016, China; e-mail: wangx118@zju.edu.cn.

Footnotes

Submitted 9 December 2021; Accepted 7 April 2022; prepublished online on Blood First Edition 19 April 2022. DOI 10.1182/blood.2021015108.

*H.W., X.H., and Lei Zhang contributed equally to this study.

†H.J., X.W., and L.L. jointly supervised this work.

RNA-Seq data are available at GEO under accession numbers GSE193832, GSE193721, and GSE193769.

The online version of this article contains a data supplement.

The publication costs of this article were defrayed in part by page charge payment. Therefore, and solely to indicate this fact, this article is hereby marked "advertisement" in accordance with 18 USC section 1734.

REFERENCES

1. Khwaja A, Bjorkholm M, Gale RE, et al. Acute myeloid leukaemia. *Nat Rev Dis Primers*. 2016;2:16010.
2. Madan V, Koeffler HP. Differentiation therapy of myeloid leukemia: four decades of development. *Haematologica*. 2021;106(1):26-38.
3. de Thé H. Differentiation therapy revisited. *Nat Rev Cancer*. 2018;18(2):117-127.
4. Amatangelo MD, Quek L, Shih A, et al. Enasidenib induces acute myeloid leukemia cell differentiation to promote clinical response. *Blood*. 2017;130(6):732-741.
5. DiNardo CD, Stein EM, de Botton S, et al. Durable remissions with ivosidenib in IDH1-mutated relapsed or refractory AML. *N Engl J Med*. 2018;378(25):2386-2398.
6. Chen L, Guo P, Zhang Y, et al. Autophagy is an important event for low-dose cytarabine treatment in acute myeloid leukemia cells. *Leuk Res*. 2017;60:44-52.
7. Sykes DB, Kfoury YS, Mercier FE, et al. Inhibition of dihydroorotate dehydrogenase overcomes differentiation blockade in acute myeloid leukemia. *Cell*. 2016;167(1):171-186.
8. Hofer A, Crona M, Logan DT, Sjöberg BM. DNA building blocks: keeping control of manufacture. *Crit Rev Biochem Mol Biol*. 2012;47(1):50-63.
9. Aye Y, Li M, Long MJ, Weiss RS. Ribonucleotide reductase and cancer: biological mechanisms and targeted therapies. *Oncogene*. 2015;34(16):2011-2021.
10. Stillman B. Deoxynucleoside triphosphate (dNTP) synthesis and destruction regulate the replication of both cell and virus genomes. *Proc Natl Acad Sci USA*. 2013;110(35):14120-14121.
11. Zhang K, Hu S, Wu J, et al. Overexpression of RRM2 decreases thrombspondin-1 and increases VEGF production in human cancer cells in vitro and in vivo: implication of RRM2 in angiogenesis. *Mol Cancer*. 2009;8(1):11.
12. Engström Y, Eriksson S, Jildevik I, Skog S, Thelander L, Tribukait B. Cell cycle-dependent expression of mammalian ribonucleotide reductase. Differential regulation of the two subunits. *J Biol Chem*. 1985;260(16):9114-9116.
13. Koppenhafer SL, Goss KL, Terry WW, Gordon DJ. Inhibition of the ATR-CHK1 pathway in ewing sarcoma cells causes DNA damage and apoptosis via the CDK2-mediated degradation of RRM2. *Mol Cancer Res*. 2020;18(1):91-104.
14. D'Angiolella V, Donato V, Forrester FM, et al. Cyclin F-mediated degradation of ribonucleotide reductase M2 controls genome integrity and DNA repair. *Cell*. 2012;149(5):1023-1034.
15. Chen L, Chen JY, Huang YJ, et al. The augmented R-loop is a unifying mechanism for myelodysplastic syndromes induced by high-risk splicing factor mutations. *Mol Cell*. 2018;69(3):412-425.e6.
16. Matos DA, Zhang JM, Ouyang J, Nguyen HD, Genois MM, Zou L. ATR protects the genome against R loops through a MUS81-triggered feedback loop. *Mol Cell*. 2020;77(3):514-527.
17. Garcia-Diaz B, Garone C, Barca E, et al. Deoxynucleoside stress exacerbates the phenotype of a mouse model of mitochondrial neurogastrointestinal encephalopathy. *Brain*. 2014;137(Pt 5):1337-1349.
18. Davenne T, Klintman J, Sharma S, et al. SAMHD1 limits the efficacy of forodesine in leukemia by protecting cells against the cytotoxicity of dGTP. *Cell Rep*. 2020;31(6):107640.

19. Franzolin E, Pontarin G, Rampazzo C, et al. The deoxynucleotide triphosphohydrolase SAMHD1 is a major regulator of DNA precursor pools in mammalian cells. *Proc Natl Acad Sci USA*. 2013;110(35):14272-14277.

20. Schneider C, Oellerich T, Baldauf H-M, et al. SAMHD1 is a biomarker for cytarabine response and a therapeutic target in acute myeloid leukemia. *Nat Med*. 2017;23(2):250-255.

21. Herold N, Rudd SG, Ljungblad L, et al. Targeting SAMHD1 with the Vpx protein to improve cytarabine therapy for hematological malignancies. *Nat Med*. 2017;23(2):256-263.

22. Fan H, Huang A, Villegas C, Wright JA. The R1 component of mammalian ribonucleotide reductase has malignancy-suppressing activity as demonstrated by gene transfer experiments. *Proc Natl Acad Sci USA*. 1997;94(24):13181-13186.

23. Rehwinkel J, Maelfait J, Bridgeman A, et al. SAMHD1-dependent retroviral control and escape in mice. *EMBO J*. 2013;32(18):2454-2462.

24. Smitheman KN, Severson TM, Rajapurkar SR, et al. Lysine specific demethylase 1 inactivation enhances differentiation and promotes cytotoxic response when combined with all-*trans* retinoic acid in acute myeloid leukemia across subtypes. *Haematologica*. 2019;104(6):1156-1167.

25. Reinhold WC, Sunshine M, Liu H, et al. CellMiner: a web-based suite of genomic and pharmacologic tools to explore transcript and drug patterns in the NCI-60 cell line set. *Cancer Res*. 2012;72(14):3499-3511.

26. Liyanage SU, Hurren R, Voisin V, et al. Leveraging increased cytoplasmic nucleoside kinase activity to target mtDNA and oxidative phosphorylation in AML. *Blood*. 2017;129(19):2657-2666.

27. Gozzini A, Rovida E, Dello Sbarba P, Galimberti S, Santini V. Butyrates, as a single drug, induce histone acetylation and granulocytic maturation: possible selectivity on core binding factor-acute myeloid leukemia blasts. *Cancer Res*. 2003;63(24):8955-8961.

28. Wang F, Travins J, DeLaBarre B, et al. Targeted inhibition of mutant IDH2 in leukemia cells induces cellular differentiation. *Science*. 2013;340(6132):622-626.

29. Shih AH, Meydan C, Shank K, et al. Combination targeted therapy to disrupt aberrant oncogenic signaling and reverse epigenetic dysfunction in *IDH2*- and *TET2*-mutant acute myeloid leukemia. *Cancer Discov*. 2017;7(5):494-505.

30. Berg SL, Blaney SM, Devidas M, et al; Children's Oncology Group. Phase II study of nelarabine (compound 506U78) in children and young adults with refractory T-cell malignancies: a report from the Children's Oncology Group. *J Clin Oncol*. 2005;23(15):3376-3382.

31. DeAngelo DJ, Yu D, Johnson JL, et al. Nelarabine induces complete remissions in adults with relapsed or refractory T-lineage acute lymphoblastic leukemia or lymphoblastic lymphoma: Cancer and Leukemia Group B study 19801. *Blood*. 2007;109(12):5136-5142.

32. Gökbuget N, Basara N, Baurmann H, et al. High single-drug activity of nelarabine in relapsed T-lymphoblastic leukemia/lymphoma offers curative option with subsequent stem cell transplantation. *Blood*. 2011;118(13):3504-3511.

33. Candoni A, Lazzarotto D, Ferrara F, et al. Nelarabine as salvage therapy and bridge to allogeneic stem cell transplant in 118 adult patients with relapsed/refractory T-cell acute lymphoblastic leukemia/lymphoma. A CAMPUS ALL study. *Am J Hematol*. 2020;95(12):1466-1472.

34. Dunsmore KP, Winter SS, Devidas M, et al. Children's Oncology Group AALL0434: a phase III randomized clinical trial testing nelarabine in newly diagnosed T-cell acute lymphoblastic leukemia. *J Clin Oncol*. 2020;38(28):3282-3293.

35. Cohen MH, Johnson JR, Massie T, et al. Approval summary: nelarabine for the treatment of T-cell lymphoblastic leukemia/lymphoma. *Clin Cancer Res*. 2006;12(18):5329-5335.

36. Lainey E, Wolfromm A, Sukkurwala AQ, et al. EGFR inhibitors exacerbate differentiation and cell cycle arrest induced by retinoic acid and vitamin D3 in acute myeloid leukemia cells. *Cell Cycle*. 2013;12(18):2978-2991.

37. Behre G, Zhang P, Zhang DE, Tenen DG. Analysis of the modulation of transcriptional activity in myelopoiesis and leukemogenesis. *Methods*. 1999;17(3):231-237.

38. Sun J, He X, Zhu Y, et al. SIRT1 activation disrupts maintenance of myelodysplastic syndrome stem and progenitor cells by restoring TET2 function. *Cell Stem Cell*. 2018;23(3):355-369.

39. Perry JM, Tao F, Roy A, et al. Overcoming Wnt-β-catenin dependent anticancer therapy resistance in leukaemia stem cells. *Nat Cell Biol*. 2020;22(6):689-700.

40. Rodriguez CO Jr, Stellrecht CM, Gandhi V. Mechanisms for T-cell selective cytotoxicity of arabinosylguanine. *Blood*. 2003;102(5):1842-1848.

41. Rodriguez CO Jr, Gandhi V. Arabinosylguanine-induced apoptosis of T-lymphoblastic cells: incorporation into DNA is a necessary step. *Cancer Res*. 1999;59(19):4937-4943.

42. Leeds JM, Slabaugh MB, Mathews CK. DNA precursor pools and ribonucleotide reductase activity: distribution between the nucleus and cytoplasm of mammalian cells. *Mol Cell Biol*. 1985;5(12):3443-3450.

43. Håkansson P, Hofer A, Thelander L. Regulation of mammalian ribonucleotide reduction and dNTP pools after DNA damage and in resting cells. *J Biol Chem*. 2006;281(12):7834-7841.

44. Zhou B, Su L, Hu S, et al. A small-molecule blocking ribonucleotide reductase holoenzyme formation inhibits cancer cell growth and overcomes drug resistance. *Cancer Res*. 2013;73(21):6484-6493.

45. Rudd SG, Tsesmetzis N, Sanjiv K, et al. Ribonucleotide reductase inhibitors suppress SAMHD1 ara-CTPase activity enhancing cytarabine efficacy. *EMBO Mol Med*. 2020;12(3):e10419.

46. Eriksson S, Munch-Petersen B, Johansson K, Eklund H. Structure and function of cellular deoxyribonucleoside kinases. *Cell Mol Life Sci*. 2002;59(8):1327-1346.

47. Theiss JC, Morris NR, Fischer GA. Pyrimidine nucleotide metabolism in L5178Y murine leukemia cells: deoxycytidine protection from deoxyguanosine toxicity. *Cancer Biochem Biophys*. 1976;1(4):211-214.

48. Homminga I, Zwaan CM, Manz CY, et al. In vitro efficacy of forodesine and nelarabine (ara-G) in pediatric leukemia. *Blood*. 2011;118(8):2184-2190.

49. Balakrishnan K, Nimmanapalli R, Ravandi F, Keating MJ, Gandhi V. Forodesine, an inhibitor of purine nucleoside phosphorylase, induces apoptosis in chronic lymphocytic leukemia cells. *Blood*. 2006;108(7):2392-2398.

50. Li Z, Chen P, Su R, et al. Overexpression and knockout of miR-126 both promote leukemogenesis. *Blood*. 2015;126(17):2005-2015.

51. Weng H, Huang H, Wu H, et al. METTL14 inhibits hematopoietic stem/progenitor differentiation and promotes leukemogenesis via mRNA m^6A modification. *Cell Stem Cell*. 2018;22(2):191-205.

52. Su R, Dong L, Li Y, et al. Targeting FTO suppresses cancer stem cell maintenance and immune evasion. *Cancer Cell*. 2020;38(1):79-96.e11.

53. Corral J, Lavenir I, Impey H, et al. An Mll-AF9 fusion gene made by homologous recombination causes acute leukemia in chimeric mice: a method to create fusion oncogenes. *Cell*. 1996;85(6):853-861.

54. Chabes A, Thelander L. Controlled protein degradation regulates ribonucleotide reductase activity in proliferating mammalian cells during the normal cell cycle and in response to DNA damage and replication blocks. *J Biol Chem*. 2000;275(23):17747-17753.

55. Zhang YW, Jones TL, Martin SE, Caplen NJ, Pommier Y. Implication of checkpoint kinase-dependent up-regulation of ribonucleotide reductase R2 in DNA damage response. *J Biol Chem*. 2009;284(27):18085-18095.

56. Rothenburger T, McLaughlin K-M, Herold T, et al. SAMHD1 is a key regulator of the lineage-specific response of acute lymphoblastic leukaemias to nelarabine. *Commun Biol*. 2020;3(1):324.

57. Kufe DW, Major PP, Egan EM, Beardsley GP. Correlation of cytotoxicity with incorporation of ara-C into DNA. *J Biol Chem*. 1980;255(19):8997-900.

58. Wisch JS, Griffin JD, Kufe DW. Response of preleukemic syndromes to continuous

infusion of low-dose cytarabine. *N Engl J Med.* 1983;309(26):1599-1602.

59. Ley TJ, Miller C, Ding L, et al; Cancer Genome Atlas Research Network. Genomic and epigenomic landscapes of adult de novo acute myeloid leukemia. *N Engl J Med.* 2013;368(22):2059-2074.

60. Wouters BJ, Löwenberg B, Erpelinck-Verschueren CA, van Putten WL, Valk PJ, Delwel R. Double CEBPA mutations, but not single CEBPA mutations, define a subgroup of acute myeloid leukemia with a distinctive gene expression profile that is uniquely associated with a favorable outcome. *Blood.* 2009;113(13):3088-3091.

61. Lam FC, Kong YW, Huang Q, et al. BRD4 prevents the accumulation of R-loops and protects against transcription-replication collision events and DNA damage. *Nat Commun.* 2020;11(1):4083.

62. Shen YJ, Le Bert N, Chitre AA, et al. Genome-derived cytosolic DNA mediates type I interferon-dependent rejection of B cell lymphoma cells. *Cell Rep.* 2015;11(3):460-473.

63. Aller P, Rius C, Mata F, et al. Camptothecin induces differentiation and stimulates the expression of differentiation-related genes in U-937 human promonocytic leukemia cells. *Cancer Res.* 1992;52(5):1245-1251.

64. Chen G, Luo Y, Warncke K, et al. Acetylation regulates ribonucleotide reductase activity and cancer cell growth. *Nat Commun.* 2019;10(1):3213.

65. Chabes AL, Pfleger CM, Kirschner MW, Thelander L. Mouse ribonucleotide reductase R2 protein: a new target for anaphase-promoting complex-Cdh1-mediated proteolysis. *Proc Natl Acad Sci USA.* 2003;100(7):3925-3929.

66. Morris EJ, Jha S, Restaino CR, et al. Discovery of a novel ERK inhibitor with activity in models of acquired resistance to BRAF and MEK inhibitors. *Cancer Discov.* 2013;3(7):742-750.

67. van der Zwet JCG, Buijs-Gladdines JGCAM, Cordo' V, et al. MAPK-ERK is a central pathway in T-cell acute lymphoblastic leukemia that drives steroid resistance. *Leukemia.* 2021;35(12):3394-3405.

68. Franzolin E, Salata C, Bianchi V, Rampazzo C. The deoxynucleoside triphosphate triphosphohydrolase activity of SAMHD1 protein contributes to the mitochondrial DNA depletion associated with genetic deficiency of deoxyguanosine kinase. *J Biol Chem.* 2015;290(43):25986-25996.

69. Arpaia E, Benveniste P, Di Cristofano A, et al. Mitochondrial basis for immune deficiency. Evidence from purine nucleoside phosphorylase-deficient mice. *J Exp Med.* 2000;191(12):2197-2208.

70. Son Y, Kim S, Chung H-T, Pae H-O. Reactive oxygen species in the activation of MAP kinases. In: Cadenas E, Packer L, eds. Methods in Enzymology, vol. 528. New York: Academic Press; 2013:27–48

71. Yokoyama N, Kim Y-J, Hirabayashi Y, et al. Kras promotes myeloid differentiation through Wnt/β-catenin signaling. *FASEB Bioadv.* 2019;1(7):435-449.

72. Pei S, Pollyea DA, Gustafson A, et al. Monocytic subclones confer resistance to venetoclax-based therapy in patients with acute myeloid leukemia. *Cancer Discov.* 2020;10(4):536-551.

73. Dorrell C, Takenaka K, Minden MD, Hawley RG, Dick JE. Hematopoietic cell fate and the initiation of leukemic properties in primitive primary human cells are influenced by Ras activity and farnesyltransferase inhibition. *Mol Cell Biol.* 2004;24(16):6993-7002.

74. Brendel C, Teichler S, Millahn A, et al. Oncogenic NRAS primes primary acute myeloid leukemia cells for differentiation. *PLoS One.* 2015;10(4):e0123181.

75. Zhang J, Wang J, Liu Y, et al. Oncogenic Kras-induced leukemogeneis: hematopoietic stem cells as the initial target and lineage-specific progenitors as the potential targets for final leukemic transformation. *Blood.* 2009;113(6):1304-1314.

76. Damnernsawad A, Kong G, Wen Z, et al. Kras is required for adult hematopoiesis. *Stem Cells.* 2016;34(7):1859-1871.

77. Guièze R, Liu VM, Rosebrock D, et al. Mitochondrial reprogramming underlies resistance to BCL-2 inhibition in lymphoid malignancies. *Cancer Cell.* 2019;36(4):369-384.e13.

78. Shalem O, Sanjana NE, Hartenian E, et al. Genome-scale CRISPR-Cas9 knockout screening in human cells. *Science.* 2014;343(6166):84-87.

79. Wei L, Lee D, Law CT, et al. Genome-wide CRISPR/Cas9 library screening identified PHGDH as a critical driver for sorafenib resistance in HCC. *Nat Commun.* 2019;10(1):4681.

80. Tzoneva G, Perez-Garcia A, Carpenter Z, et al. Activating mutations in the NT5C2 nucleotidase gene drive chemotherapy resistance in relapsed ALL. *Nat Med.* 2013;19(3):368-371.

81. Meyer JA, Wang J, Hogan LE, et al. Relapse-specific mutations in NT5C2 in childhood acute lymphoblastic leukemia. *Nat Genet.* 2013;45(3):290-294.

82. Tzoneva G, Dieck CL, Oshima K, et al. Clonal evolution mechanisms in NT5C2 mutant-relapsed acute lymphoblastic leukaemia. *Nature.* 2018;553(7689):511-514.

83. Dieck CL, Tzoneva G, Forouhar F, et al. Structure and mechanisms of NT5C2 mutations driving thiopurine resistance in relapsed lymphoblastic leukemia. *Cancer Cell.* 2018;34(1):136-147.e6.

84. Unni AM, Harbourne B, Oh MH, et al. Hyperactivation of ERK by multiple mechanisms is toxic to RTK-RAS mutation-driven lung adenocarcinoma cells. *eLife.* 2018;7:7.

85. Shojaee S, Caeser R, Buchner M, et al. Erk negative feedback control enables pre-B cell transformation and represents a therapeutic target in acute lymphoblastic leukemia. *Cancer Cell.* 2015;28(1):114-128.

86. Jeffrey KL, Camps M, Rommel C, Mackay CR. Targeting dual-specificity phosphatases: manipulating MAP kinase signalling and immune responses. *Nat Rev Drug Discov.* 2007;6(5):391-403.

87. Li W, Köster J, Xu H, et al. Quality control, modeling, and visualization of CRISPR screens with MAGeCK-VISPR. *Genome Biol.* 2015;16(1):281.

88. Molina G, Vogt A, Bakan A, et al. Zebrafish chemical screening reveals an inhibitor of Dusp6 that expands cardiac cell lineages. *Nat Chem Biol.* 2009;5(9):680-687.

89. Herold N, Rudd SG, Sanjiv K, et al. SAMHD1 protects cancer cells from various nucleoside-based antimetabolites. *Cell Cycle.* 2017;16(11):1029-1038.

90. Marinello J, Chillemi G, Bueno S, Manzo SG, Capranico G. Antisense transcripts enhanced by camptothecin at divergent CpG-island promoters associated with bursts of topo-isomerase I-DNA cleavage complex and R-loop formation. *Nucleic Acids Res.* 2013;41(22):10110-10123.

91. Hamperl S, Bocek MJ, Saldivar JC, Swigut T, Cimprich KA. Transcription-replication conflict orientation modulates R-loop levels and activates distinct DNA damage responses. *Cell.* 2017;170(4):774-786.

92. Baumgartner C, Toifl S, Farlik M, et al. An ERK-dependent feedback mechanism prevents hematopoietic stem cell exhaustion. *Cell Stem Cell.* 2018;22(6):879-892.

93. Leung GP, Feng T, Sigoillot FD, et al. Hyperactivation of MAPK signaling is deleterious to RAS/RAF-mutant melanoma. *Mol Cancer Res.* 2019;17(1):199-211.

94. Neubauer A, Maharry K, Mrózek K, et al. Patients with acute myeloid leukemia and RAS mutations benefit most from postremission high-dose cytarabine: a Cancer and Leukemia Group B study. *J Clin Oncol.* 2008;26(28):4603-4609.